Integration of rock joint roughness into the Mohr-Coulomb shear behaviour model – application to dam safety analysis

Adrien Rulliere, Laurent Peyras, Jérôme Duriez, Patrice Rivard, Pierre Breul

Integration of rock joint roughness into the Mohr-Coulomb shear behaviour model – Application to dam safety analysis

Adrien RULLIERE [a], Laurent PEYRAS *[a], Jérôme DURIEZ [a], Patrice RIVARD [b] and Pierre BREUL [c]

[a] *INRAE, Aix-Marseille Univ, RECOVER, Aix-en-Provence, France*

[b] *Department of Civil Engineering, Université de Sherbrooke, Sherbrooke, QC, Canada*

[c] *Université Clermont Auvergne, Clermont-Ferrand, France*

* *corresponding author: laurent.peyras@inrae.fr*

ABSTRACT

Based on a previous experimental study that we conducted on granite joint replicas including thirty direct shear tests, this article proposes to integrate the joint roughness in the Mohr-Coulomb shear behaviour model (MC). The model integrates joint roughness into constitutive stress-displacement relationships describing mechanical behaviour of rock joint. The shear strength of rock joint is assessed by the MC shear criterion that takes into account the apparent cohesion. This MC model integrating rock joint roughness component is validated against other experimental results from the literature. It is able to accurately predict the peak shear strength of an unbounded rock joint with an average relative error of 7.9%. It is finally used to assess the role of joint roughness on the shear behaviour of a gravity dam foundation.

KEYWORDS

Apparent cohesion, DEM, Mohr-Coulomb model, rock joint, roughness, shear behaviour

Introduction

The shear strength of unbounded (cohesionless) rock joints have been extensively studied since the 1950s. For such a joint, it is widely accepted that shear strength and behaviour are controlled by many parameters such as joint roughness (Patton 1966; Barton and Choubey 1977; Kulatilake et al. 1995), joint interlocking (Zhao 1997a, 1997b), rock weathering (Barton and Choubey 1977; Nouailletas et al. 2017), joint mechanical properties (Ghazvinian et al. 2010; Rullière et al. 2021) and scale (Bandis et al. 1981; Tatone and Grasselli 2013; Buzzi and Casagrande 2018).

Several failure criteria have been developed to predict joint peak shear strength. The simplest one is the linear Mohr-Coulomb criterion that links the joint peak shear strength (τ_{peak}) to the normal load (σ_N) and joint surface characteristics (C and φ). Barton and Choubey (1977) extended the joint surface characteristic parameter φ of the Mohr-Coulomb criterion to take into account the effects of joint roughness and joint weathering on peak shear strength. Barton-Choubey criterion is well known in rock mechanics (ISRM 2014). This criterion introduces the joint roughness parameter (JRC) determined by visual comparison of the joint with a two-dimensional abacus. Because this abacus cannot cover the wide spectrum of roughness that a joint can exhibit, some authors consider that the JRC value might be prone to subjectivity (Hsiung et al. 1993; Beer, Stead, and Coggan 2002; D. Sow et al. 2016; D. Sow et al. 2017).

Later, Grasselli and Egger (2003) proposed a more complex criterion which adopts a three-dimensional view of the rock joint to estimate its peak shear strength. The criterion proposed by Grasselli and Egger (2003) considers that only the asperities facing the shear direction contribute to joint peak shear strength. Nevertheless, it was demonstrated that this criterion tends to overestimate the peak shear strength of smooth joints ((Xia et al. 2014). More recently, Zhang et al. (2016) proposed a 2D criterion that considers only a proportion of the asperities facing the shear direction. Wang and Lin

53 (2018) proposed a shear criterion that describes either the sliding or shearing mechanism
54 effects on peak shear strength as a function of the normal stress. Others relevant
55 references in the field of our work have to be cited also (Chen et al. 2022; Wang et al.
56 2022; Zhang et al. 2022a; Zhan et al 2022b; Barton and Shen 2017; Wang et al. 2020).
57 Besides assessing the shear strength of joints, it is necessary to evaluate their pre-
58 failure shear behaviour. To this end, several shear behaviour models that analytically
59 describe the interactions between stresses and relative displacements of a joint subjected
60 to shearing have been developed. Historically, the work of Goodman, Taylor, and Brekke
61 (1968) is considered as the first development of numerical laws to model the shear
62 behaviour of rock joints. It suggests that stresses are connected to displacements through
63 mathematical linear elastic laws using constant stiffness, the shear stress being bounded
64 by a maximum value that can be estimated using one of the criteria mentioned above.
65 Later, considerable research improved this model either by considering that stiffness is
66 not systematically constant during shearing (Bandis et al. 1983) or by taking into account
67 the effect of joint damage (Cundall and Lemos 1988). The continuous improvement of
68 computers has led to the development of even more complex and comprehensive shear
69 behaviour models in recent decades. Duriez et al. (2011) developed a shear behaviour
70 model with incrementally non-linear constitutive relations to describe the mechanical
71 behaviour of infilled rock joints along a variety of loading paths. Oh et al. (2015) and Li
72 et al. (2016) proposed a model that considers together and independently the contributions
73 of large-scale roughness (waviness) and small-scale roughness (unevenness) of a joint to
74 its shear behaviour.
75 For engineering applications such as rock slope stability and dam foundation
76 design, many engineering guidelines suggest using the Mohr-Coulomb criterion to assess
77 the shear strength of a rock joint (USBR 1987; US Army Corps of Engineers 1995; CFBR

2012; ISRM 2014; Federal Energy Regulatory Commission 2016). Mohr-Coulomb input parameters, cohesion C and friction angle φ, are determined through experimental shear tests on small joint samples. For an unbounded rock joint, the cohesion obtained corresponds to the apparent cohesion concept, which depicts the roughness and joint interlocking effect on the shear strength (Amitrano and Schmittbuhl 2002; Rullière et al. 2020). However, guidelines recommend a safe practice considering a low or null value of apparent cohesion, since its extrapolation to the scale of the structure is delicate. But this safe practice is conservative since the resistance characteristics of the joint due to its morphology (roughness, interlocking) are neglected.

The aim of this article is to integrate rock joint roughness components into the Mohr-Coulomb shear behaviour model which is chosen for its wide usage in engineering practice strength (USBR 1987; US Army Corps of Engineers 1995; CFBR 2012; ISRM 2014; Federal Energy Regulatory Commission 2016), in order to take into account the role of joint roughness on joint shear behaviour. This integration aims to take into account the role of joint roughness on joint shear behaviour and is built up on the base of thirty-five experimental tests (direct joint shear tests and joint compression tests) and links joint roughness to joint shear behaviour and strength. The rock joint shear behaviour is described through stress-displacement laws. Joint failure state is expressed by the Mohr-Coulomb criterion including the apparent cohesion concept, to stick to the current practice of rock engineering. At the end, the MC shear behaviour model integrating rock joint roughness is validated with experimental data coming from rock mechanics literature.

The paper is divided into four parts. The first part presents the materials and methods (Part 1). In the second part, the MC shear behaviour model integrating rock joint roughness is developed and calibrated (Part 2). It consists in the development of empirical laws correlating the joint roughness to the shear behaviour model input parameters. These

empirical laws are then integrated in the MC model, so that it takes into account the role of joint roughness on joint shear behaviour. In the third part, the developed model is validated in the third part: model blind-predictions are faced to direct shear test results from rock mechanics literature in order to evaluate the model's accuracy (Part 3). In the last part, the MC shear behaviour model integrating rock joint roughness is used to demonstrate the key role of joint roughness on the shear behaviour of a gravity dam foundation (Part 4). All the numerical calculations presented in this paper were performed using the Discrete Element Method (DEM).

1. Materials and Methods

This part presents: i) the experimental data used to develop the empirical equations linking the joint roughness to the shear behaviour model input parameters, ii) the shear behaviour model used in the study, and iii) the DEM code in which the model will be implemented to predict the shear behaviour at the laboratory and gravity dam scales.

1.1.Experimental data used to develop the shear behaviour model

The experimental data come from a previous work (Rullière et al. 2020) and are summarized in this article. Thirty direct shear tests on granite joint replicas were carried out in CNL conditions and under 0.1, 0.2, 0.35 and 0.6 MPa normal stress. Additional joint compression tests were conducted to characterize the joint normal stiffness. The tests were specifically performed for the research work presented in this paper.

It is specified in this introduction to the experimental data that our work does not take into account the scale effect between the sample tested in the laboratory and the real scale model. Several authors such as (Bandis et al. 1981) have worked on the scale effect and have shown the influence of sample size on shear strength. This question of scale

126 effect between laboratory and field is, in general, a universal problem of this kind of study
127 that our research has not taken into account.

128 *1.1.1. Joint roughness statistical indicator (Z_2)*

129 Many studies have been conducted to define the roughness concept because it is
130 considered to be the main parameter governing the shear behavior of rock discontinuities.
131 Barton and Choubey (1977) developed the joint roughness coefficient (JRC) to estimate
132 joint roughness using a visual comparison of 10 standard profiles. With the advancement
133 of non-contact methodologies used to scan rock joint surfaces, new parameters have been
134 developed to assess roughness. In this context, the 2D directional parameter Z_2 is widely
135 accepted and used in the rock mechanics community as a non-subjective roughness
136 indicator (Tse and Cruden 1979; Kulatilake et al. 1995; Tatone and Grasselli 2010;
137 Magsipoc, Zhao, and Grasselli 2019; Ram and Basu 2019). Indeed, for a joint profile, the
138 parameter Z_2 is a 2D directional parameters that describes the local topographic slope of
139 the joint profile. Z_2 can be seen as a topographical slope and corresponds to the root-
140 mean-square of the first derivative (Myers 1962). Z_2 can be calculated as:

141 $$Z_2 = \left[\frac{1}{L}\sum_{1}^{n-1}\left(\frac{y_{i+1}-y_i}{x_{i+1}-x_i}\right)^2\right]^{\frac{1}{2}} \quad (1)$$

142 Where L is the length of the joint profile, x_i and y_i are the coordinates of the
143 discretized joint profile (0.5 mm sampling interval).

144 The calculation of Z_2 requires only a topographic scan of the joint surface and, in
145 comparison to other roughness indicators, it is rather simple and non-time-consuming to
146 implement the calculation of Z_2 in an algorithm.

147 Five granite joints (J0, J1, J2, J3, J4) with different roughness's (Z_2 from 0 to
148 0.373) were selected to produce the replicas. Prior to replica production, the granite joints
149 were scanned with a non-contact laser profilometer (Figure 1). Data from the scans were

150 then implemented in a specifically designed algorithm linking the surface morphology to
151 the roughness statistical parameter Z_2 (Rullière et al. 2020). Table 1 shows the Z_2 value
152 for each of the five granite joints used to produce the replicas.

153 [FIGURE 1 HERE]

154 [TABLE 1 HERE]

155 *1.1.2. Direct shear test*

156 Following the production of the replica (six replicas per selected roughness), thirty direct
157 shear tests were conducted in CNL conditions. Twenty direct shear test results, carried
158 out on J0, J1, J2, J3 and J4 under 0.1, 0.2, 0.35 and 0.6-MPa normal stress come from the
159 results of Rullière et al. (2020). For this work, ten additional direct shear tests were carried
160 out for J0, J1, J2, J3 and J4, under 0.1 and 0.6-MPa. These new results provide more shear
161 tests results over the 0.1 to 0.6-MPa interval and strengthen the Mohr-Coulomb failure
162 envelope plot. The normal stress levels used in this study correspond to those observed
163 in dam foundations or other civil engineering works (Sow et al. 2017). Each replica was
164 used for a single direct shear test.

165 Figure 2 shows the shear strength versus shear displacement curves for all the
166 direct shear tests used in this study. The key data are summarized in Table 2. It classically
167 appears from the direct shear tests results that the rougher the joint, the higher the shear
168 strength (peak or residual).

169 [FIGURE 2 HERE]

170 [TABLE 2 HERE]

171 Figure 3 depicts the Mohr-Coulomb failure envelopes plotted from the
172 experimental direct shear test results for the peak and residual shear strengths. Apparent
173 cohesion and friction angle values at both peak and residual stages are shown in Table 1.
174 Again, it appears that the rougher the joint, the higher the apparent cohesion and friction

175 angle values. Since the results were obtained on an unbounded rock joint replica, it was
176 considered that the apparent cohesion could be mobilized at peak stage only (EPRI 1990;
177 Rullière et al. 2020). Therefore, $C_{APP\ Residual}$ = 0-kPa.

178 [FIGURE 3 HERE]

179 The shear stiffness K_S was calculated for shear stresses ranging from 25 to 75%
180 of the peak shear strength (Kumar and Verma 2016). This precaution allows setting aside
181 the curved areas of the shear strength-shear displacement curve (initial loading and peak
182 phase). Table 1 presents the K_S mean value obtained for all the joints tested. It appears
183 that the rougher the joint, the higher the shear stiffness.

184 Figure 4 shows normal versus shear displacement curves for all the direct shear
185 tests (Rullière et al. 2020). It is verified that the dilatant behaviour depends on both of the
186 joint roughness and the normal stress imposed during the shear tests. As shown in Figure
187 4, a rougher joint lead to larger normal displacement during a direct shear test in CNL
188 conditions. The dilatancy angle (dN) is calibrated from the maximal value of the Δ_V / Δ_U
189 ratio (usually around the peak shear displacement value). Table 1 shows the dN mean
190 value obtained for all the joints tested. As expected, the rougher the joint, the higher the
191 dilatancy angle.

192 [FIGURE 4 HERE]

193 *1.1.3. Compression test results*

194 Joint normal stiffness (K_N) assessment requires specific experimental tests called joint
195 compression test (Bandis et al. 1981; Fan, Cao, and Tang 2018). Such a test involves
196 recording the relative normal displacements of a rock joint under a given normal load
197 (Figure 5).

198 [FIGURE 5 HERE]

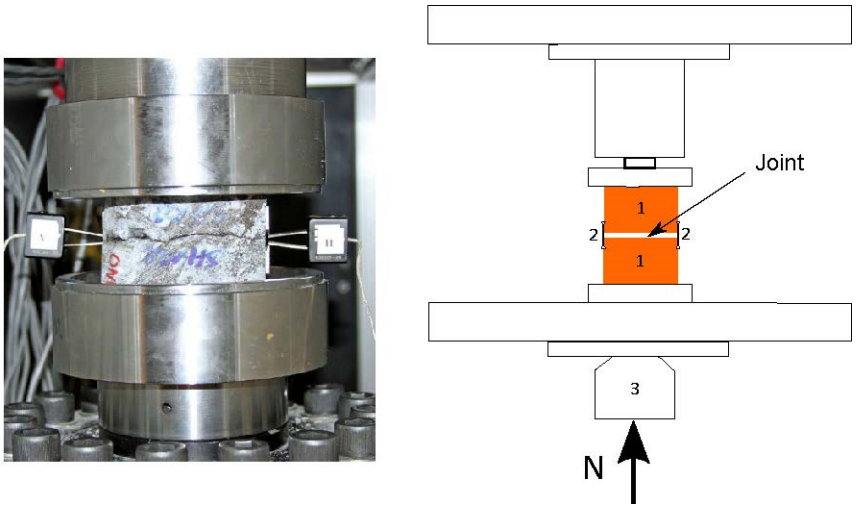

In practice, several loading-unloading cycles are performed to determine the normal stiffness of a rock joint (Bandis et al. 1983; Marache 2002). The first cycle allows the joint to be fully interlocked, so that the deformations recorded during the following cycles correspond to the joint's deformations only and not to a change of joint interlocking.

Five joint compression tests were performed, for each granite joint. The joints were subjected to an increasing normal stress, up to 30% of the compressive strength matrix of the material, prior to a progressive discharge. The charge-discharge cycles were repeated three times and the K_N was measured along the last loading cycle. Figure 6 shows the normal stress versus normal displacement curves obtained from the joint compression tests. The K_N value of each joint is presented in Table 1. If the K_N values are compared to joint roughness, it seems that the rougher a joint, the higher the K_N.

[FIGURE 6 HERE]

1.2. Shear behaviour model used in the study

The shear behaviour model used in this study follows an elastic-plastic formulation based on the work of Goodman, Taylor, and Brekke (1968). As a joint is subjected to a shear stress, the response of the joint is initially exclusively elastic. The displacements can be

correlated to the normal or shear stress variations through constant joint normal or shear stiffness and classical linear elastic laws:

$$\begin{pmatrix} d\sigma_N \\ d\tau \end{pmatrix} = \begin{pmatrix} K_N & 0 \\ 0 & K_S \end{pmatrix} . \begin{pmatrix} d\Delta_V \\ d\Delta_U \end{pmatrix} \quad (2)$$

Where $d\sigma_N$ is the normal stress variations, $d\tau$ is the shear stress variation, K_N is the joint normal stiffness, K_S is the joint shear stiffness, $d\Delta_U$ is the shear displacement increment and $d\Delta_V$ is the normal displacement increment.

A direct shear test conducted in Constant Normal Load (CNL) conditions is piloted by constant tangential displacement increments ($d\Delta_U$). Therefore, the shear stress progressively increases according to (2). On the contrary, the normal stress increment is null. In this type of test, this means that the model assumes no normal displacement increments ($d\Delta_V$) during the elastic stage.

The elastic stage extends until the shear stress τ reaches the shear strength value τ_{peak} defined by the Mohr-Coulomb criterion which serves as both a (constant) yield surface and plastic limit condition in the (τ;σ_N) plane, in the absence of elasto-plastic hardening. As rock joints are unbounded, the cohesion of the Mohr-Coulomb criterion corresponds to the apparent cohesion, C_{app}, as presented in the introduction.

$$\tau = C_{app} + \sigma_N.\tan(\varphi) \quad (3)$$

Where τ is the shear stress, σ_N is the normal stress, C_{app} is the apparent cohesion and φ is the friction angle.

As soon as the peak shear stress is reached, the shear behaviour model considers that the joint is in a failure phase: the elastic stage is completed and the plastic stage begins. The shear stress decreases instantaneously to the residual and constant value $\tau_{residual}$. This choice of a brittle behaviour, as opposed to a gradual softening, is chosen for simplicity, in line with engineering practices.

In the plastic stage, a flow rule governs the dilatancy whereby normal displacement variations are correlated to shear displacement variations and to the joint dilatancy angle:

$$d\Delta_V = d\Delta_U.\tan(dN) \quad (4)$$

Where $d\Delta_U$ is the shear displacement increment, $d\Delta_V$ is the normal displacement increment and dN the dilatancy angle.

1.3.The Discrete Element Method

A rock mass can be considered as a set of rocky blocks separated from each other by joints. For such a set, a mechanical stress will lead to displacements that are almost exclusively due to the displacements along the joints (the rocky block deformations are considered as insignificant). This consideration exactly matches the DEM hypothesis: blocks are considered as infinitely stiff and the displacements are exclusively due to block contacts.

The DEM method and UDEC software (Itasca 2019) were used in this paper to perform the different numerical calculations, either to simulate laboratory direct shear tests in CNL conditions or to assess the shear behaviour of a gravity dam founded on a complex jointed rock mass. In UDEC, the hydro-mechanical behaviour of a set of blocks and joints is simulated by adjusting the joint properties (mechanical properties and behaviour models).

2. Calibration of the MC shear behaviour model integrating rock joint roughness

2.1. Equations linking joint roughness to shear behaviour model input parameters

The aim of this section is to develop empirical equations that correlate the joint roughness to the input parameters of the MC shear behaviour model integrating rock joint roughness. These input parameters are $C_{app\ peak}$, φ_{peak}, $C_{app\ residual}$, $\varphi_{residual}$, dN, K_N and Ks (see section 1 for more details). The experimental data presented in Part 1 are used and three kinds of mathematical laws are studied: linear, power, and exponential laws. For each kind of law, the least square method was used to determine coefficients *a*, *b* and *c* :

$$P = a \,.\, Z_2 + b \tag{5}$$

$$P = a \,.\, Z_2^{\,b} + c \tag{6}$$

$$P = a \,.\, e^{\,Z_2 . x} + c \tag{7}$$

Where *a*, *b* and *c* are empirical coefficients and P stands for any model parameters among $C_{app\ peak}$, φ_{peak}, $C_{app\ residual}$, $\varphi_{residual}$, dN, K_N and K_S.

For the sake of concision, only the power equations are presented. Indeed, it appeared during the study that the power equations (6) were able to correlate the joint roughness to the shear behaviour input parameter with great precision. In comparison to linear and exponential equations, the power equations had the highest coefficient of determination (R^2). However, the reader will find linear and exponential equations in Appendix A.

Based on the data presented in Table 1, the power law equations describing the shear behaviour and shear failure state of the joint are developed. Power law coefficients

a, *b* and *c*, which correlate the roughness to the peak apparent cohesion, peak friction angle, residual friction angle, dilatancy angle, and normal and shear stiffness, are presented in Table 3. Figures 7 to 9 compare the power law predictions to the experimental data.

The values of coefficients *a, b* and *c* and the equations developed in this section are valid only for the following conditions:

- the rock joint roughness is described by the Z_2 statistical parameter. Z_2 ranges between 0 (smooth joint) and 0.373 (rough joint);
- the rock joint is subjected to a normal load ranging from 0.1 to 0.6-MPa.

[TABLE 3 HERE]

[FIGURE 7 HERE]

[FIGURE 8 HERE]

[FIGURE 9 HERE]

2.2.*Numerical direct shear tests using the MC shear behaviour model*

Once the shear behaviour model was established, thirteen numerical direct shear tests were performed under the exact same conditions of normal load and roughness as the experimental direct shear tests presented in the previous section. In other words, data provided by the numerical shear behaviour model were compared to the experimental data used to develop it, to control if the numerical results fit the experimental observations and if the calibration of the numerical model had been carried out well.

Using UDEC software (Itasca 2019), the rock joint is represented by the contact between two infinitely rigid blocks. While the lower block is fixed, the upper block is subjected to both a normal load and a constant horizontal displacement rate. In the DEM model, the lower block length is longer than the upper block to avoid any toppling of the

upper block. For the numerical direct shear tests, the normal load and horizontal displacement rate were set as equal to the experimental values applied during the experimental direct shear tests (normal load ranges from 0.1 to 0.6-MPa and the horizontal displacement rate is 0.1 mm/min to insure quasi-staticity). The numerical model also required the roughness of the joint (depicted by Z_2).

Figure 10 and Figure 11 show the shear stress versus horizontal displacement curves and normal displacement versus horizontal displacement curves. The dotted lines correspond to the experimental data, while the full lines correspond to the numerical results.

From Figures 10 and 11, it appears that despite its bilinear aspect, the numerical model manages to describe the rock joint shear behaviour efficiently. This is particularly true during the peak phase, and to a lesser extent for the residual phase (end of test). Nonetheless, as shown in Figure 10, the post-peak joint behaviour is not realistically described by the shear behaviour model since as soon as the peak shear strength is reached, the release of the shear stress is instantaneous, while the experimental tests show a progressive decrease of the shear stress towards a residual shear stress value. Figure 11 shows that the shear behaviour model satisfactorily reproduces the dilatant behaviour of a rock joint, although there is no contraction stage and for the shear behaviour model, the dilatancy starts as soon as the shear stress reaches its peak (these are related to the equations that govern the MC shear behaviour model, see Part 1). However, it should be noted that in rock-mechanics engineering practice, the post-peak shear behaviour has not been extensively studied and the MC model approximations could be sufficient for a vast majority of applications.

Figure 12 displays the model peak and residual shear strength and contrasts it with the experimental recorded values. For the peak stage, the results predicted by the model

333 are very close to the experimentally recorded values (generally, the difference is less than
334 10%). For the residual phase, the differences are slightly larger, but can be explained by
335 the numerous jumps present on the experimental curves (Figure 2).
336
337 [FIGURE 10 HERE]
338 [FIGURE 11 HERE]
339 [FIGURE 12 HERE]
340 The shear behaviour model can be considered as calibrated, as the numerical shear
341 test results matches the experimental results.
342 The next step consists of a validation in which we aim to assess the ability of the
343 shear behaviour model to predict the rock joint shear behaviour of all rock joints. To this
344 end, the aim of the next section is to compare the model blind-predictions to other
345 published experimental direct shear test results that were not used to develop the
346 numerical model.

347 3. Validation of the MC shear behaviour model with literature data

348 *3.1.Published data used for the validation step*

349 We consider four articles in the rock mechanics literature that present experimental direct
350 shear tests carried out in the validity conditions of the shear behaviour model developed
351 in this study. In these four studies, the joint roughness indicator (Z_2) ranges between 0
352 and 0.373 and joints were subjected to normal load ranging from 0.1 to 0.6-MPa during
353 the direct shear tests (Lee, Park, and Song 2014; Jang and Jang 2015; Li et al. 2018; Ram
354 and Basu 2019). Please note that the data from these studies were not used to develop the
355 numerical model previously described.

Ram and Basu (2019) studied the shear behaviour of unfilled natural rock joints with reference to the weathering grade of the joint. Due to the different weathering grade used by the authors, only seven direct shear tests results could be used (Table 4). These shear tests were carried out on smooth rock joints (Z_2 ranges from 0.057 to 0.130) under a normal stress of about 0.2-MPa.

Jang and Jang (2015) conducted more than 180 direct shear tests on rock joint replicas. Forty direct shear test results could be used directly in this research paper: Z_2 ranges from 0.082 to 0.351 and the normal stresses levels are 0.2 and 0.53-MPa MPa (Table 4).

From Lee, Park, and Song (2014), six direct shear tests results were extracted: Z_2 ranges from 0.142 to 0.253 and the normal stress levels range from 0.1 to 0.5-MPa (Table 4).

Lastly, in Li et al. (2018), only one direct shear test was conducted in the conditions presented above ($Z_2 < 0.373$ and the normal load from 0.1 to 0.6-MPa).

In brief, this amounts to fifty-four direct shear results selected from several published rock mechanics papers that were used to validate the shear behaviour model developed in this paper. The selected direct shear tests were carried out at various normal stress levels (from 0.1 to 0.53-MPa) on natural rock joints or on rock joint replicas that exhibited several levels of roughness (Z_2 ranging from 0.057 to 0.351). All of the selected papers gave the peak shear strength, whereas only eleven residual shear strengths were available.

3.2.Results

Table 4 and Figure 13 compare the experimental direct shear tests results from literature to the shear behaviour model blind-predictions. In Table 4, the relative difference between experimental results and model blind-predictions are also given.

Except for some cases that will be discussed, it appeared that the model developed is able to accurately predict the peak shear strength τ_{peak} of a natural rough rock joint subjected to low normal stress levels: a mean relative error of 12.0% is observed, and even 7.9% if some results are left out (Table 4). For example, joint N2000-J13 from the study of Jang and Jang (2015) exhibited an intermediate roughness (Z_2 = 0.21). Experimental peak shear strength was 0.412 MPa at 0.2MPa normal stress and 0.893 MPa at 0.53 MPa normal stress. In the exact same conditions of roughness, the shear behaviour model predicted a peak shear strength of 0.423 MPa and 0.943 MPa at 0.2 MPa and 0.53 MPa of normal stress. This represents a relative difference of 3% at 0.2 MPa normal stress and 6% at 0.53 MPa normal stress.

Regarding the residual shear strength (τ_r), a mean relative difference of 23% was obtained between the experimental results and the shear behaviour model blind-predictions (Table 4).

[TABLE 4 HERE]

[FIGURE 13 HERE]

3.3.Discussion

Regarding the peak shear strength (τ_{peak}), most of the model blind-predictions matched the experimental results although we observed some data with large differences (see dashed circles in Figure 13). In our opinion, the few large differences observed between the model blind-predictions and some very specific experimental data were linked to rock type. Indeed, during a direct shear test, a rock joint could exhibit different shear mechanisms such as sliding or shearing that can take place on the joint surface at the same time, depending on rock type, rock joint roughness and normal load (Rullière et al. 2020).

In our study, the shear behaviour model developed was based on granite joints, which are known to exhibit a "*slickenside to rough undulating roughness*" in accordance

406 with the ISRM (1978) description. In Rullière et al. (2020), the granite joints exhibited
407 mainly sliding mechanisms during the direct shear tests. On the other hand, in the study
408 of Jang and Jang (2015), the rock joints came from different rock types including granite
409 and schist joints, which are described being "*very rough and stepped*" in accordance with
410 the ISRM (1978). Very rough or stepped asperities will tend to gather the shear stresses
411 during a direct shear test, and schist joints will mainly be damaged by shearing
412 mechanisms. The reader should note that the direct shear tests conducted in (Lee, Park,
413 and Song 2014; Li et al. 2018; Ram and Basu 2019) were carried out on granite and gneiss
414 joints. In Jang and Jang (2015), as the rock type was not linked to the joint identification
415 code, it is therefore impossible to know which rock joint replica came from granite or
416 schists joints. Nevertheless, we attributed the large difference between the experimental
417 data and the model blind-predictions to the rock type (schist), as explained above. If the
418 specific large differences of Jang and Jang (2015) are excluded (see dashed circles in
419 Figure 13), the mean relative error between the experimental data from the rock
420 mechanics literature and the model blind-predictions is 7.9%.

421 Regarding the residual shear strength (τ_r), a mean relative difference of 23% was
422 obtained between the experimental results and the model blind-predictions (Table 4).
423 Although this mean relative difference is based on a few experimental results, as not all
424 the selected papers gave the residual shear strength, this gap between the experimental
425 data and the model blind-prediction can be explained by the following reasons:

426 • The model approach to predicting the residual shear strength is very conservative.
427 The shear stress decreases suddenly to its residual value once the peak is reached
428 whereas during an experimental direct shear test, the shear stress decreases
429 gradually to its residual value,

- Also, during this progressive shear stress decrease observed in the experimental tests, some shear stress jumps could be observed, very likely related to sheared material that interfered between the joint walls.

Finally, it appeared that the MC shear behaviour model integrating rock joint roughness was able to accurately predict the experimental peak shear strength of various direct shear tests published in the rock mechanics literature. For some specific cases, the blind-predictions were quite far from the experimental results, but in our opinion these differences can be explained by the rock type. Indeed, the shear behaviour model was developed using granite joints while some of the data presented were related to schist joints.

4. Application of the MC shear behaviour model to a gravity dam

Gravity dams are mainly exposed to shear mechanisms: under the combination of different actions, shearing can take place at the rock-concrete interface or at rock mass foundation joints. International gravity dam design guidelines suggest using the Mohr-Coulomb criterion to assess the shear strength of a rock joint of such structures (USBR 1987; US Army Corps of Engineers 1995; CFBR 2012; Federal Energy Regulatory Commission 2016).

Part 3 showed that the shear strength and behaviour of a rough rock joint subjected to low normal stresses could be accurately estimated by the numerical shear behaviour model developed, which takes into account joint roughness (developed in Part 2). In this Part 4, we wish to highlight: i) that the shear behaviour model developed previously could be used at the dam scale, and ii) the influence of the rock joint roughness on the shear behaviour of a gravity dam, subjected to different load cases.

4.1.Presentation of the numerical gravity dam model and hypothesis

The gravity dam studied is founded on a granitic rock mass from Canadian shield, intersected by three sets of joints that are prone to discontinuities in the displacement field, i.e. finite relative displacements across themselves. Among these sets, one is sub-horizontal and two sub-vertical, presenting dips of 16° N 0°, 80° N 0° and 82° N 180°, respectively. The joints of the same set are spaced according to a uniform distribution, whose standard deviations and mean values are given in Table 5. The persistence of the joints was considered as fully persistent (default preset). This agrees with the observations of the drillings carried out on the dam site, in the context of a dam founded on the Canadian shield where the persistence is generally very high.

All the joints exhibited the same roughness characteristics, described by a Z_2 value. In the following calculations, the Z_2 value was increased from zero (depicting a smooth joint) to 0.373 (depicting a very rough rock joint). It was also assumed that the rock mass joints are very long compared with the dam size and they can be considered as persistent at the numerical study scale. In other words, the joints we that the joints cut the entire rock foundation mass. There is therefore no increase in the length of the joints. On the other hand, the joints are free to open. The granite density was set to 2500 kg/m^3.

[TABLE 5 HERE]

The specifications of the case study gravity dam are:

- Height of 45m and an operating level of 41 m;
- The width at the head of the structure is 4 m;
- The upstream face is vertical, while the downstream batter (H/V) is 0.65;
- The width at the toe is 32 m.

The dam is fully made of concrete (density of 2350 kg/m^3) and it is assumed that its construction was of good quality: rock-foundation and construction interfaces were treated. In other words, excellent adhesion can be considered for concrete-concrete construction joints and rock-concrete interfaces. Therefore, relative displacements can only occur in the rock mass, along the rock joints described previously. For the sake of convenience, it was also assumed that the gravity dam was not equipped with any drainage system. Figure 14 shows a schematic view of the gravity dam modelled on its granitic rock mass foundation.

[FIGURE 14 HERE]

The numerical model is built using UDEC software (Itasca 2019) with a Discrete Element Method (DEM) approach. The DEM makes it straightforward to describe the discontinuity of displacements across joints, while a continuous-based FEM approach would require to adopt a more complex model, typically XFEM (Moës et al., 1999). In this DEM model, the particles are blocks of different sizes and shapes that come from three sets of discontinuities that cut the granitic massif. Numerical damping was used with a 0.8 coefficient and the time step was fixed at 30 μs to avoid divergence of the explicit dynamic scheme. The boundaries of the numerical model were fixed in all directions and located at a distance of at least five times the structure height to avoid any interferences.

Different load cases were considered:

(1) Normal Operating Conditions: the reservoir is filled;
(2) Extreme Conditions: the reservoir is filled and the dam is subjected to a seismic solicitation.

In Normal Operating Conditions, the dam is only subjected to mechanical actions related to the presence of water upstream of the structure (water pressure on the upstream

face of the dam, uplift). The reservoir is instantly filled with water from the natural foundation ground to the normal operating level (41 m of water upstream, 0 m of water downstream). The hydrostatic pressure field is imposed on the gravity dam rock foundation joints and assumed to be constant in time.

The seismic calculation is performed using a simple pseudo-static method, as suggested by French regulations. The values of the horizontal (a_h) and vertical acceleration (a_v) are: $a_h = 2.0$ m/s^2 and $a_v = 1.8$ m/s^2.

For the two loading cases considered, the analysis of the behaviour of the structure is carried out based on horizontal and vertical displacements of: i) the dam downstream face crest, and ii) the dam foundation at a depth of 3 m below the upstream toe.

4.2.Results and discussion

Table 6 shows the displacements recorded during the numerical modelling of a gravity dam subjected to load levels. From Table 6, it appears that the rock joint roughness has an important effect on the horizontal displacements recorded at the dam crest or in its foundation. However, the effect of rock joint roughness on the vertical displacements is not obvious.

For smooth rock foundation joints ($Z_2 = 0$), when the dam is filled and without seismic solicitation, the horizontal and vertical displacements recorded at the dam crest reach respectively a value of 17.2 mm and -0.74 mm. When seismic solicitation is applied, the displacements at the dam crest increase and reach the values of 24.5 mm for the horizontal displacement and 2.21 mm for the vertical displacement (Table 6).

For the rough rock foundation joints ($Z_2 = 0.373$), the horizontal displacements observed at the crest under normal operations and seismic conditions are reduced in comparison to smooth joints. Under normal operating conditions, the horizontal dam crest displacements reach the value of 11.00 mm maximum versus 17.2 mm for smooth joints,

i.e. a difference of 36% (Table 6). Under seismic conditions, the same trend can be observed: horizontal dam crest displacements reach a value of 19.00 mm versus 24.5 mm for smooth joints, i.e. a difference of 22% (Table 6). Figure 15 clearly shows that the horizontal displacements recorded at the dam crest (under normal operating and seismic conditions) decrease linearly when the rock joint roughness increases.

The largest displacements were observed at the crest of the structure; they are the consequence of displacements of the rock discontinuities located inside the rock mass foundation, as depicted in Figure 16. In Table 6 and Figure 17, it can also be seen that as the rock joint roughness increases, the horizontal displacement recorded below the dam upstream toe decreases linearly.

[TABLE 6 HERE]

[FIGURE 15 HERE]

[FIGURE 16 HERE]

[FIGURE 17 HERE]

Therefore, the application of the MC shear behaviour model integrating rock joint roughness to the gravity dam scale illustrates the important role of rock joint roughness in the shear behaviour of the dam. This influence of roughness was considered through the shear behaviour model input parameters. It appeared that displacement linearly decrease with an increase of rock foundation joint roughness (Z_2 value), either at dam crest or in its foundation (normal operation and extreme conditions).

Conclusion

The aim of this study was to develop a practical shear behaviour model, based on the Mohr-Coulomb model, which depicts the role of joint roughness on joints shear behaviour. The MC shear behaviour model integrating rock joint roughness included

551 constitutive stress-displacement laws. The model shear failure corresponded to the Mohr-
552 Coulomb criterion including apparent cohesion.

553 The shear behaviour model was developed based on more than thirty-five
554 experimental tests (direct shear tests and compression tests). Power laws that correlated
555 the joint roughness parameter Z_2 to the shear behaviour input parameter were developed
556 (calibration step, Part 2). The model was then validated by comparing its blind-
557 predictions to publish experimental data (validation step, Part 3). The results indicated
558 that the MC shear behaviour model integrating rock joint roughness was able to predict
559 the peak shear strength of an unbounded rock joint with an average relative error of 7.9%).
560 The shear behaviour model developed was found to be strongly influenced by the rock
561 type.

562 Lastly, the shear behaviour model developed was applied at full scale (gravity
563 dam) to highlight the role of rock joint roughness in dam shear behaviour. This practical
564 application exhibited that the higher the rock joint roughness (Z_2 value), the smaller the
565 displacements (either at the dam crest or in its foundations).

566 Regarding the perspectives of this work, it is important to recall that the MC shear
567 behaviour model integrating rock joint roughness is valid for specific conditions: a normal
568 load from 0.1 to 0.6-MPa and a roughness indicator Z_2 ranging from 0 to 0.373. Moreover,
569 the shear behaviour model developed takes into account the effects of joint roughness on
570 its shear strength and behaviour. However, the reader should know that other parameters
571 could also have strong effects (rock properties, interlocking, contact properties, the
572 presence of infilled materials in joints, etc.).

573 Future work will attempt to incorporate other shear behaviour / strength influence
574 parameters in the shear behaviour model developed. However, this task requires much
575 more data and implies launching new experimental and exhaustive studies. Finally, it is

576 important to note that the last part of this paper is intended to be only explanatory since
577 the tests were conducted at the laboratory scale. Thus, more work is required to use the
578 shear behaviour model developed accurately at a larger scale.

579 **Acknowledgments**

580 The authors are grateful to the National Sciences and Engineering Research
581 Council of Canada (NSERC), Hydro-Québec and INRAE (France) for funding the
582 project. We thank Danick Charbonneau and Ghislaine Luc for their technical help during
583 the experimental project.

584 **References**

585 Amitrano, D., and Schmittbuhl, J. 2002. “Fracture Roughness and Gouge Distribution
586 of a Granite Shear Band.” *Journal of Geophysical Research: Solid Earth* 107
587 (B12): 1–16. https://doi.org/10.1029/2002JB001761.

588 Bandis, S.C, Lumsden, A., and Barton, N.R. 1981. “Experimental Studies of Scale
589 Effects on the Shear Behaviour of Rock Joints.” *International Journal of Rock*
590 *Mechanics and Mining Sciences & Geomechanics Abstracts* 18 (1): 1–21.
591 https://doi.org/10.1016/0148-9062(81)90262-X.

592 Bandis, S.C., Lumsden, A.C., Barton, N.R. 1983. “Fundamentals of Rock Joint
593 Deformation.” *International Journal of Rock Mechanics and Mining Sciences &*
594 *Geomechanics Abstracts* 20 (6): 249–68. https://doi.org/10.1016/0148-
595 9062(83)90595-8.

596 Barton Nick, Shen Baotang. 2017. "Risk of shear failure and extensional failure around
597 over-stressed excavations in brittle rock". *Journal of Rock Mechanics and*
598 *Geotechnical Engineering.* Volume 9, Issue 2, April 2017, 210-225.

https://doi.org/10.1016/j.jrmge.2016.11.004

Barton, N., and V. Choubey. 1977. “The Shear Strength of Rock Joints in Theory and Practice.” *Rock Mechanics* 10 (1–2): 1–54. https://doi.org/10.1007/BF01261801.

Beer, A. J., D. Stead, and J. S. Coggan. 2002. “Technical Note Estimation of the Joint Roughness Coefficient (JRC) by Visual Comparison.” *Rock Mechanics and Rock Engineering* 35 (1): 65–74. https://doi.org/10.1007/s006030200009.

Buzzi, O, and D Casagrande. 2018. “A Step towards the End of the Scale Effect Conundrum When Predicting the Shear Strength of Large in Situ Discontinuities.” *International Journal of Rock Mechanics and Mining Sciences*, 2018. https://doi.org/10.1016/j.ijrmms.2018.01.027.

CFBR. 2012. “Recommandations Pour La Justification de La Stabilité Des Barrages-Poids.”

Chen Bing, Shen Baotang, Jiang Haiyang. 2022. "Shear behavior of intact granite under thermo-mechanical coupling and three-dimensional morphology of shear-formed fractures". *Journal of Rock Mechanics and Geotechnical Engineering*. https://doi.org/10.1016/j.jrmge.2022.04.006

Cundall, P. A., and J Lemos. 1988. “Numerical Simulation of Fault Instabilities with the Continuously-Yielding Joint Model.” In *PROCEEDINGS OF THE 2ND INTERNATIONAL SYMPOSIUM ON ROCKBURSTS AND SEISMICITY IN MINES*, edited by C Fairhurst. Minneapolis: Balkema Rotterdam. https://doi.org/10.1016/0148-9062(85)92069-8.

Duriez, J., Darve, F., and Donzé, F.-V.. 2011. “A Discrete Modeling-Based Constitutive

621 Relation for Infilled Rock Joints." *International Journal of Rock Mechanics and*
622 *Mining Sciences* 48 (3): 458–68. https://doi.org/10.1016/j.ijrmms.2010.09.008.

623 EPRI. 1990. "Uplift Pressures, Shear Strengths, and Tensile Strengths for Stability
624 Analysis of Concrete Gravity Dams."

625 Fan, Wenchen, Ping Cao, and Guodong Tang. 2018. "Experimental and Numerical
626 Study on the Damage Evolution of Random Rock Joint Surface During Direct
627 Shear Under CNL Condition." *Geotechnical and Geological Engineering* 37 (2):
628 975–83. https://doi.org/10.1007/s10706-018-0664-y.

629 Federal Energy Regulatory Commission. 2016. "Gravity Dams." In *Engineering*
630 *Guidelines for the Evaluation of Hydropower Projects*, 3.1–3.39.

631 Ghazvinian, A. H., A. Taghichian, Mahmoud Hashemi, and S. A. Mar'ashi. 2010. "The
632 Shear Behavior of Bedding Planes of Weakness Between Two Different Rock
633 Types with High Strength Difference." *Rock Mechanics and Rock Engineering* 43
634 (1): 69–87. https://doi.org/10.1007/s00603-009-0030-8.

635 Goodman, RE, RL Taylor, and TL Brekke. 1968. "A Model for the Mechanics of
636 Jointed Rock." *Journal of the Soil Mechanics and Foundation Division ASCE*
637 14:637–659.

638 Grasselli, G., and Egger, P. 2003. "Constitutive Law for the Shear Strength of Rock
639 Joints Based on Three-Dimensional Surface Parameters." *International Journal of*
640 *Rock Mechanics and Mining Sciences* 40 (1): 25–40.
641 https://doi.org/10.1016/S1365-1609(02)00101-6.

642 Hsiung, S.M., Ghosh, A., Ahola, M P., and Chowdhury, A.H. 1993. "Assessment of

643 Conventional Methodologies for Joint Roughness Coefficient Determination."
644 *International Journal of Rock Mechanics and Mining Sciences And* 30 (7): 825–29.
645 https://doi.org/10.1016/0148-9062(93)90030-H.

646 ISRM. 1978. "International Society for Rock Mechanics Commission on
647 Standardization of Laboratory and Field Tests. Suggested Methods for the
648 Quantitative Description of Discontinuities in Rock Masses." *International Journal*
649 *of Rock Mechanics and Mining Sciences and Geomechanics Abstracts* 15 (6): 319–
650 68. https://doi.org/10.1016/0148-9062(78)91472-9.

651 Ulusay, R. 2014. *The ISRM Suggested Methods for Rock Characterization, Testing and*
652 *Monitoring: 2007-2014*. Ed. Springer International Publishing.
653 https://doi.org/10.1007/978-3-319-07713-0.

654 Itasca. 2019. *UDEC - Universal Distinct Element Code - User Manual*. Minneapolis:
655 Itasca Consulting Group.

656 Jacobsson, L., Flansbjer, M., and Andersson, L. 2016. "Normal Loading and Shear
657 Tests on Rock Joints from Olkiluoto" 31 (June).

658 Jang, Hyun-Sic, and Bo-An Jang. 2015. "New Method for Shear Strength
659 Determination of Unfilled, Unweathered Rock Joint." *Rock Mechanics and Rock*
660 *Engineering* 48 (4): 1515–34. https://doi.org/10.1007/s00603-014-0660-3.

661 Kulatilake, P.H.S.W., Shou, G., Huang, T.H., and Morgan, R.M. 1995. "New Peak
662 Shear Strength Criteria for Anisotropic Rock Joints." *International Journal of Rock*
663 *Mechanics and Mining Sciences & Geomechanics Abstracts* 32 (7): 673–97.
664 https://doi.org/10.1016/0148-9062(95)00022-9.

665 Kumar, Rakesh, and Abhiram Kumar Verma. 2016. “Anisotropic Shear Behavior of
666 Rock Joint Replicas.” *International Journal of Rock Mechanics and Mining*
667 *Sciences* 90 (December): 62–73. https://doi.org/10.1016/j.ijrmms.2016.10.005.

668 Lee, Yong-Ki, Jung-Wook Park, and Jae-Joon Song. 2014. “Model for the Shear
669 Behavior of Rock Joints under CNL and CNS Conditions.” *International Journal*
670 *of Rock Mechanics and Mining Sciences* 70 (September): 252–63.
671 https://doi.org/10.1016/j.ijrmms.2014.05.005.

672 Li, Oh, Mitra, and Hebblewhite. 2016. “A Constitutive Model for a Laboratory Rock
673 Joint with Multi-Scale Asperity Degradation.” *Computers and Geotechnics* 72:
674 143–51. https://doi.org/10.1016/j.compgeo.2015.10.008.

675 Li, Yuanhui, Leibo Song, Quan Jiang, Chengxiang Yang, Chang Liu, and Bing Yang.
676 2018. “Shearing Performance of Natural Matched Joints with Different Wall
677 Strengths under Direct Shearing Tests.” *Geotechnical Testing Journal* 41 (2):
678 20160315. https://doi.org/10.1520/GTJ20160315.

679 Magsipoc, Earl, Qi Zhao, and Grasselli, G.. 2019. “2D and 3D Roughness
680 Characterization.” *Rock Mechanics and Rock Engineering*, no. 0123456789.
681 https://doi.org/10.1007/s00603-019-01977-4.

682 Marache, A. 2002. “Comportement Mécanique d’une Fracture Rocheuse Sous
683 Contraintes Normale et Tangentielle.” École Centrale des Arts et Manufactures
684 « École Centrale Paris ».

685 Moës, N., Dolbow, J. and Belytschko, T. 1999. "A finite element method for crack
686 growth without remeshing." *Int. J. Numer. Meth. Engng.* 46: 131-150,
687 https://doi.org/10.1002/(SICI)1097-0207(19990910)46:1<131::AID-

688 NME726>3.0.CO;2-J

689 Myers, N.O. 1962. “Characterization of Surface Roughness.” *Wear* 5 (3): 182–89.
690 https://doi.org/10.1016/0043-1648(62)90002-9.

691 Nouailletas, O., C. Perlot, P. Rivard, G. Ballivy, and C. La Borderie. 2017. “Impact of
692 Acid Attack on the Shear Behaviour of a Carbonate Rock Joint.” *Rock Mechanics*
693 *and Rock Engineering* 50 (6): 1439–51. https://doi.org/10.1007/s00603-017-1182-
694 6.

695 Oh, J, E J Cording, and T Moon. 2015. “A Joint Shear Model Incorporating Small-Scale
696 and Large-Scale Irregularities.” *International Journal of Rock Mechanics and*
697 *Mining Sciences* 76: 78–87. https://doi.org/10.1016/j.ijrmms.2015.02.011.

698 Patton, FD. 1966. “Multiple Modes of Shear Failure In Rock.” In *1st ISRM Congress*.
699 Lisbon: International Society for Rock Mechanics.

700 Ram, B. K., and A. Basu. 2019. “Shear Behavior of Unfilled-Planar Quartzitic Rock
701 Joints with Reference to Weathering Grade of Joint Surfaces.” *Rock Mechanics*
702 *and Rock Engineering* 52 (10): 4113–21. https://doi.org/10.1007/s00603-019-
703 01815-7.

704 Rullière, A., Rivard, P., Peyras, L., Breul, P. 2020. “Influence of Roughness on the
705 Apparent Cohesion of Rock Joints at Low Normal Stresses.” *Journal of*
706 *Geotechnical and Geoenvironmental Engineering* 146 (3): 1–15.
707 https://doi.org/10.1061/(ASCE)GT.1943-5606.0002200.

708 Rulliere, A., Rivard, P., Peyras, L., Breul, P. 2021. “Influence of Material Strength on
709 the Apparent Cohesion of Unbounded Gravity Dam Joints under Low Normal Stress.”

Journal of Geotechnical and Geoenvironmental Engineering 147(10). DOI: 10.1061/(ASCE)GT.1943-5606.0002608.

Sow, D., P. Rivard, L. Peyras, P. Breul, Z. A. Moradian, C. Bacconnet, and G. Ballivy. 2016. "Comparison of Joint Shearing Resistance Obtained with the Barton and Choubey Criterion and with Direct Shear Tests." *Rock Mechanics and Rock Engineering* 49 (8): 3357–61. https://doi.org/10.1007/s00603-015-0898-4.

Sow, D., Carvajal, C., Breul, P., Peyras, L., Rivard, P., Bacconnet, C., and Ballivy, G.. 2017. "Modeling the Spatial Variability of the Shear Strength of Discontinuities of Rock Masses: Application to a Dam Rock Mass." *Engineering Geology* 220: 133–43. https://doi.org/10.1016/j.enggeo.2017.01.023.

Tatone, Bryan S.A., and Grasselli, G. 2010. "A New 2D Discontinuity Roughness Parameter and Its Correlation with JRC." *International Journal of Rock Mechanics and Mining Sciences* 47 (8): 1391–1400. https://doi.org/10.1016/j.ijrmms.2010.06.006.

Tatone, Bryan S A, and Grasselli, G. 2013. "An Investigation of Discontinuity Roughness Scale Dependency Using High-Resolution Surface Measurements." *Rock Mechanics and Rock Engineering* 46 (4): 657–81. https://doi.org/10.1007/s00603-012-0294-2.

Tse, R, and Cruden, D.M. 1979. "Estimating Joint Roughness Coefficients." *International Journal of Rock Mechanics and Mining Sciences & Geomechanics Abstracts* 16 (5): 303–7. https://doi.org/10.1016/0148-9062(79)90241-9.

US Army Corps of Engineers. 1995. *Gravity Dam Design*. *USACE Engineer Manual*. 1st ed. Washington: DEPARTMENT OF THE ARMY U.S. Army Corps of

Engineers. http://oai.dtic.mil/oai/oai?verb=getRecord&metadataPrefix=html&identifier=ADA402909.

USBR. 1987. *Design of Small Dams*. Edited by A Water Resources Technical Publication. *UNITED STATES DEPARTMENT OF THE INTERIOR BUREAU OF RECLAMATION - A Water Resources Technical Publication*. 3rd ed.

Wang Luyu, Vuik Cornelis, Hajibeygi Hadi. 2022. "A stabilized mixed-FE scheme for frictional contact and shear failure analyses in deformable fractured media". E*ngineering Fracture Mechanics,* Vol. 267, 15 May 2022. https://doi.org/10.1016/j.engfracmech.2022.108427

Wang Luyu, Chen Weizhong, Tan Xuyan, Tan Xianjun, Yang Jianping, Yang Diansen & Zhang Xi. 2020. "Numerical investigation on the stability of deforming fractured rocks using discrete fracture networks: a case study of underground excavation". Bu*lletin of Engineering Geology and the Environment,* 79, 133–151. https://doi.org/10.1007/s10064-021-02233-2

Wang, Hu, and Hang Lin. 2018. “Non-Linear Shear Strength Criterion for a Rock Joint with Consideration of Friction Variation.” *Geotechnical and Geological Engineering* 36 (6): 3731–41. https://doi.org/10.1007/s10706-018-0567-y.

Xia, Cai-Chu, Zhi-Cheng Tang, Wei-Min Xiao, and Ying-Long Song. 2014. “New Peak Shear Strength Criterion of Rock Joints Based on Quantified Surface Description.” *Rock Mechanics and Rock Engineering* 47 (2): 387–400. https://doi.org/10.1007/s00603-013-0395-6.

Zhang Qi, Yan Xia, Li Zihao. 2022a. "A mathematical framework for multiphase

poromechanics in multiple porosity media". *Computers and Geotechnics.* Vol. 146, June 2022. https://doi.org/10.1016/j.compgeo.2022.104728

Zhang Qi, Wang Ze-Yu, Yin Zhen-Yu, Jin Yin-Fu. 2022b. "A novel stabilized NS-FEM formulation for anisotropic double porosity media". C*omputer Methods in Applied Mechanics and Engineering.* Vol. 401, Part B, 1 Nov. 2022, https://doi.org/10.1016/j.cma.2022.115666

Zhang, Xiaobo, Qinghui Jiang, Na Chen, Wei Wei, and Xixia Feng. 2016. "Laboratory Investigation on Shear Behavior of Rock Joints and a New Peak Shear Strength Criterion." *Rock Mechanics and Rock Engineering* 49 (9): 3495–3512. https://doi.org/10.1007/s00603-016-1012-2.

Zhao, J. 1997a. "Joint Surface Matching and Shear Strength Part A: Joint Matching Coefficient (JMC)." *International Journal of Rock Mechanics and Mining Sciences* 34 (2): 173–78. https://doi.org/10.1016/S0148-9062(96)00062-9.

Zhao, J. 1997b. "Joint Surface Matching and Shear Strength Part B: JRC-JMC Shear Strength Criterion." *International Journal of Rock Mechanics and Mining Sciences* 34 (2): 179–85. https://doi.org/10.1016/S0148-9062(96)00063-0.

Appendix A

Linear laws correlating the Z_2 value to the shear behaviour model input parameters.

$$K_N = 31.22 \cdot x + 68.14 \qquad R^2 = 0.96 \qquad (8)$$

$$K_S = 4.91 \cdot x + 1.96 \qquad R^2 = 0.77 \qquad (9)$$

$$C_{app\ peak} = 821.9 \cdot x - 28.5 \qquad R^2 = 0.88 \qquad (10)$$

$$\varphi_{peak} = 118.5 \cdot x + 28.06 \qquad R^2 = 0.96 \qquad (11)$$

779 $\varphi_{residual} = 89.6 \cdot x + 25.6$ $R^2 = 0.98$ (12)

780 $dN = 79.55 \cdot x + 0.26$ $R^2 = 0.99$ (13)

781 Exponential laws correlating the Z_2 value to the shear behaviour model input parameters.

782 $K_N = 15.87 \cdot e^{1.49 \cdot x} + 52.61$ $R^2 = 0.97$ (14)

783 $K_S = 0.257 \cdot e^{5.77 \cdot x} + 1.90$ $R^2 = 0.94$ (15)

784 $C_{app\ peak} = 56.64 \cdot e^{5.09 \cdot x} - 55.01$ $R^2 = 0.99$ (16)

785 $\varphi_{peak} = 1.164x10^4 \cdot e^{0.011 \cdot x} - 1.164x10^4$ $R^2 = 0.96$ (17)

786 $\varphi_{residual} = 1.081x10^4 \cdot e^{0.006 \cdot x} - 1.081x10^4$ $R^2 = 0.96$ (18)

787 $dN = 1.809x10^4 \cdot e^{0.0041 \cdot x} - 1.809x10^4$ $R^2 = 0.98$ (19)

Detailed answers to the reviewers

Integration of rock joint roughness into the Mohr-Coulomb shear behaviour model – Application to dam safety analysis

Authors: Adrien RULLIERE, Laurent PEYRAS, Jérôme DURIEZ, Patrice RIVARD and Pierre BREUL

European Journal of Environmental and Civil Engineering

N° remark	Remark	Answer
	Reviewer 1	
1	The quality of figures is still bad and some figures are even blurry	We are very sorry about the quality of the figures that was lost during the generation of the PDF file. The figures have been taken out of the text and attached in vector PDF format. The quality is much better now. Again, we are sorry for this problem.
	Reviewer 2	
1	In Section "Material and Methods", the experimental results should be provided firstly, then introduce the MC model and DEM.	Done
2	The references cited in introduction should be up to date. Please refer to the relevant literature 10.1007/s10064-019-01536-9 ; 10.1016/j.jrmge.2022.04.006 10.1016/j.engfracmech.2022.108427 ; 10.1016/j.jrmge.2016.11.004	Done. These references have been added.
3	Some figures are not in high quality, for instance, the fonts in Figs 2, 6, 10, 11 and 13 … are too small to difficult to identify. It is kindly suggested that improving the quality.	Done. See the answer to the question n°1 – reviewer n°1
4	Eq (3). The explanation of symbols should be in an academic style.	Done, see reviewer 3 question 3.
5	Eq (7) "Z2" should be subscript.	Done
6	Some of the subtitles of subsections should be more concise and clearer.	Done. Several subtitles have been changed and shortened.
7	Please unify the term "rock joint" and "shear strength of rock joint"	Done. We have change all the “rock joint shear strength” by “shear strength of rock joint”
Corrections suggested on the PDF File		We thank the reviewer for his careful proofreading which improves the article All the corrections suggested have been taken into account.

Reviewer 3		
1	The figure quality is extremely bad	See the answer to the question n°1 – reviewer n°1
2	Do you think your model could apply to the kilometer scale? If so, how? If not, why?	We do not think that the model could apply to the kilometer scale, due to the scale effect. The model considers the roughness provided by the joint asperities (micro and macroscale), but it does not take into account the waviness of the joint. In the introduction of § 1.1, we say on this subject: *"It is specified in this introduction to the experimental data that our work does not take into account the scale effect between the sample tested in the laboratory and the real scale model. Several authors such as (Bandis et al. 1981) have worked on the scale effect and have shown the influence of sample size on shear strength. This question of scale effect between laboratory and field is, in general, a universal problem of this kind of study that our research has not taken into account."*
3	Please learn how to embed a mathematical equation in Word professional. I have attached a file for you to learn (together with high-resolution figures).	Thanks for the comment. We modified the equations in the manuscript and the explanation of symbols are now in an academic style.
4	Why do you prefer the Mohr-Coulomb model to the Drucker-Prager model? Have you considered strain-softening in your analysis? Please refer to the following papers, discuss them, and include them in your reference list. DOI: 10.1016/j.compgeo.2022.104728 DOI: 10.1016/j.cma.2022.115666	We use the Mohr-Coulomb model because it is the model that is most widely used in the world in dam engineering to assess the stability of dams. We mentioned this in the introduction: " *The aim of this article is to integrate rock joint roughness components into the Mohr-Coulomb shear behaviour model which is chosen for its wide usage in engineering practice strength (USBR 1987; US Army Corps of Engineers 1995; CFBR 2012; ISRM 2014; Federal Energy Regulatory Commission 2016), in order to take into account the role of joint roughness on joint shear behaviour*." The Drucker-Prager model is not so used in dam engineering. We considered a brittle deformation-damping in our MC model since, during the numerical shear test, the shear stress reaches a maximum value before a sudden drop to a residual value. Done. These references have been added.
5	Do you consider the propagation (dynamics) of joints?	The joints were considered persistent at the scale of the model, which means that the joints cut the whole rock mass foundation. There is therefore no increase in the length of the joints. On the other hand, the joints are free to open. These details were already into the paper: please see lines 459-462 and 466-468. We added some details to be more understandable. Please see lines 468-470.

Table 1. Experimental data obtained for each joint studied.

Joint	Joint roughness statistical indicator Z_2	Apparent cohesion at peak shear strength C_{APP_Peak} (kPa)	Friction angle at peak shear strength φ_{Peak} (°)	Apparent cohesion at residual shear strength $C_{APP\_Residual}$ (kPa)	Friction angle at residual shear strength $\varphi_{residual}$ (°)	Dilatancy angle dN (°)	Joint normal stiffness K_N (GPa/m)	Joint shear stiffness K_S (GPa/m)
J0	0	0	25.6	0	25.6	0	68.5	2.2
J1	0.186	95	54.0	0	40.7	15.3	73.8	2.4
J2	0.241	140	58.7	0	49.1	20.6	74.4	3.2
J3	0.302	202	62.8	0	54.6	22.9	78.4	3.3
J4	0.373	326	69.9	0	57.5	30.2	80.0	4.1

Table 2. Direct shear test results

Joint	σ_N (MPa)	τ_{peak} (MPa)	$\tau_{residual}$ (MPa)
J0	0.10	0.04	0.04
	0.20	0.09	0.09
	0.35	0.17	0.17
	0.60	0.32	0.32
J1	0.10	0.24	0.11
	0.10	0.26	0.07
	0.20	0.41	0.20
	0.35	0.52	0.38
	0.60	0.94	0.59
	0.60	1.02	0.47
J2	0.10	0.31	0.11
	0.10	0.32	0.14
	0.20	0.52	0.22
	0.35	0.68	0.43
	0.60	1.34	0.73
	0.60	1.05	0.75
J3	0.10	0.39	0.22
	0.20	0.60	0.37
	0.35	1.00	0.61
	0.60	1.42	0.96
	0.60	1.41	0.76
J4	0.10	0.61	0.21
	0.10	0.58	0.15
	0.20	1.02	0.43
	0.35	1.22	0.51
	0.60	1.93	0.94
	0.60	2.20	1.06

Table 3. Power law coefficients a, b and c values according to the input parameter of interest.

Shear behaviour model input parameter	*a*	*b*	*c*
$C_{app\ peak}$	2120.0	1.93	2.81
φ_{peak}	82.17	0.64	25.62
$C_{app\ residual}$	0.0	0.0	0.0
$\varphi_{residual}$	87.39	0.98	25.45
dN	75.0	0.94	0.02
K_N	39.82	1.24	58.50
K_S	15.55	2.12	2.17

Table 4: Comparison of experimental direct shear test results from the rock mechanics literature (Lee, Park, and Song 2014; Jang and Jang 2015; Li et al. 2018; Ram and Basu 2019) and the numerical blind-predictions of the shear behaviour model developed in this paper - all values are in MPa. The results in italics have been left aside for future work.

				Experimental data		**Shear behaviour model blind-predictions**		**%**	
Reference	**Sample ID**	**Z_2**	**σ_N**	**τ_{peak}**	**τ_R**	**τ_{peak}**	**τ_R**	**τ_{peak}**	**τ_R**
Ram and Basu (2019)	JS-15	0.057	0.23	0.22	0.20	0.20	0.14	**8.5**	**31.4**
	JS-19	0.130	0.23	0.49	0.28	0.31	0.18	**36.5**	**37.2**
	JS-21	0.057	0.23	0.19	0.15	0.20	0.14	**5.7**	**8.7**
	JS-26	0.047	0.24	0.19	0.15	0.20	0.14	**3.1**	**8.0**
	JS-30	0.130	0.23	0.34	0.24	0.31	0.18	**8.6**	**26.8**
	JS-33	0.084	0.23	0.23	0.20	0.24	0.15	**3.8**	**24.6**
	JS-34	0.061	0.22	0.23	0.20	0.20	0.13	**13.9**	**33.5**
Li et al. (2018)	J3	0.235	0.27	0.66	0.50	0.60	0.29	**8.9**	**42.8**
Jang and Jang (2015)	N2000-J1	0.082	0.20	0.23	-	0.21		**10.1**	**-**
			0.53	0.56	-	0.52		**8.0**	**-**
	N2000-J2	0.118	0.20	0.26	-	0.26		**1.0**	**-**
			0.53	0.62	-	0.62		**0.1**	**-**
	N2000-J3	0.127	0.20	0.33	-	0.27		**16.8**	**-**
			0.53	0.73	-	0.65		**10.7**	**-**
	N2000-J4	0.126	0.20	0.27	-	0.27		**1.5**	**-**
			0.53	0.64	-	0.65		**1.0**	**-**
	N2000-J5	0.132	0.20	0.28	-	0.28		**0.3**	**-**
			0.53	0.65	-	0.66		**3.0**	**-**
	N2000-J6	0.139	0.20	0.35	-	0.29		**17.3**	**-**
			0.53	0.79	-	0.69		**12.5**	**-**
	N2000-J7	0.147	0.20	0.33	-	0.30		**8.3**	**-**
			0.53	0.76	-	0.71		**6.5**	**-**
	N2000-J8	0.161	0.20	0.35	-	0.33		**4.7**	**-**

			0.53	0.79	-	0.76		**3.9**	**-**
	N2000-J9	0.154	0.20	0.32	-	0.32		**0.4**	**-**
			0.53	0.75	-	0.74		**1.7**	**-**
	N2000-J10	*0.178*	*0.20*	*0.50*	-	*0.36*		***28.0***	**-**
			0.53	*1.03*	-	*0.82*		***20.4***	**-**
	N2000-J11	0.179	0.20	0.35	-	0.36		**4.5**	**-**
			0.53	0.78	-	0.82		**5.6**	**-**
	N2000-J12	0.189	0.20	0.36	-	0.38		**7.1**	**-**
			0.53	0.80	-	0.86		**7.8**	**-**
	N2000-J13	0.210	0.20	0.41	-	0.42		**2.7**	**-**
			0.53	0.89	-	0.94		**5.7**	**-**
	N2000-J14	0.221	0.20	0.42	-	0.45		**6.7**	**-**
			0.53	0.91	-	0.99		**8.7**	**-**
	N2000-J15	0.218	0.20	0.38	-	0.44		**15.4**	**-**
			0.53	0.84	-	0.98		**15.9**	**-**
	N2000-J16	0.224	0.20	0.43	-	0.46		**7.0**	**-**
			0.53	0.90	-	1.01		**12.0**	**-**
	N2000-J17	0.241	0.20	0.44	-	0.50		**11.8**	**-**
			0.53	0.98	-	1.08		**11.1**	**-**
	N2000-J18	0.247	0.20	0.43	-	0.51		**18.7**	**-**
			0.53	0.93	-	1.11		**19.2**	**-**
	N2000-J19	*0.327*	*0.20*	*0.56*	-	*0.75*		***34.1***	**-**
			0.53	*1.15*	-	*1.58*		***36.7***	**-**
	N2000-J20	*0.350*	*0.20*	*0.57*	-	*0.84*		***48.0***	**-**
			0.53	*1.19*	-	*1.75*		***47.3***	**-**
Lee, Park and Song (2014)	R-463	0.142	0.20	0.28	-	0.29		**5.3**	**-**
	R-1130	0.227	0.10	0.29	0.10	0.29	0.10	**0.6**	**1.6**
			0.20	0.35	-	0.46		**32.1**	**-**
	R-1233	0.244	0.20	0.42	0.29	0.50	0.22	**19.9**	**25.2**
			0.50	0.96	0.50	1.04	0.55	**9.3**	**9.3**
	R-1284	0.253	0.20	0.57	-	0.53		**7.6**	**-**

Table 5. Geological data for the joints of the gravity dam rock foundation.

Joint set	Dip angle	Mean spacing (m)	Standard deviation on spacing (m)
1	16° N 0°	0.95	0.37
2	80° N 0°	1.52	0.82
3	82° N 180°	2.33	1.77

Table 6. Displacement values recorded during the numerical application at the gravity dam scale of the shear behaviour model developed. Values are in mm.

Z_2	Normal operating conditions				Seismic conditions			
	Crest horizontal disp	Toe horizontal disp	Crest vertical disp	Toe vertical disp	Crest horizontal disp	Toe horizontal disp	Crest vertical disp	Toe vertical disp
0	17.2	13.8	-0.7	-2.4	24.5	18.1	2.2	-2.2
0.05	17.9	8.8	1.5	-2.4	29.2	12.8	4.6	-2.5
0.1	19.3	8.1	-2.2	-2.2	19.8	8.3	2.6	-2.2
0.15	16.5	6.9	1.7	-2.3	28.2	10.1	5.5	-2.5
0.2	15.1	6.8	1.4	-2.4	25.4	9.0	4.8	-2.4
0.25	13.8	7.5	1.0	-2.1	23.1	8.9	4.0	-2.0
0.3	12.9	6.6	0.8	-2.6	21.3	7.9	3.6	-2.4
0.373	11.0	5.9	0.3	-2.8	19.0	7.2	2.8	-2.6

Figure 1: 3D view of the granite joints used in this study (Rullière et al. 2020).

Figure 2: Shear stress versus shear displacement curves from Rullière et al. (2020).

Figure 3: Mohr-Coulomb linear regression at peak and residual state for the five granite joints used in this study.

Figure 4: normal displacement versus shear displacement curves from Rullière et al. (2020).

Figure 5: Photograph (Jacobsson, Flansbjer, and Andersson 2016) and schematic view of the hydraulic press during the compression tests. The rock joint sample (1) is set in a uniaxial press controlled for displacements. During the joint compression test, extensometers (2) and a load cell (3) record the normal relative displacements and the normal force (N).

Figure 6: Compression test curves for all the granite joints used in this study.

Figure 7: Comparison between the experimental data and empirical power law predictions for apparent cohesion, peak friction angle and residual friction angle.

Figure 8: Comparison between the experimental data and empirical power law predictions for the dilatancy angle.

Figure 9: Comparison between the experimental data and empirical power law predictions for normal and shear stiffness.

Figure 10: Joint shear stress versus shear displacement curves according to: i) in solid lines the model predictions, and ii) in dotted lines the experimental data from Rullière et al. (2020).

Figure 11: Joint normal displacement versus shear displacement curves according to: i) in solid lines the model predictions, and ii) in dotted lines the experimental data from Rullière et al. (2020).

Figure 12: Comparison of experimental direct shear test results and the numerical results of the shear behaviour model developed in this paper

Figure 13: Comparison between the model blind-predictions for peak shear strength and experimental data. Arrows show the largest differences between the model and experimental data.

Figure 14: schematic view of the gravity dam model.

Figure 15: Horizontal displacements recorded at the dam crest for each Z_2 value used during the numerical calculations. The normal operation conditions are shown in blue, the extreme condition in red.

Figure 16: Global displacements (in m) recorded on the gravity dam under seismic conditions for Z_2 =0.1.

Figure 17: horizontal displacements recorded at the upstream toe of the dam for each Z_2 value used during the numerical calculations. The normal operation conditions are shown in blue, the extreme condition in red.

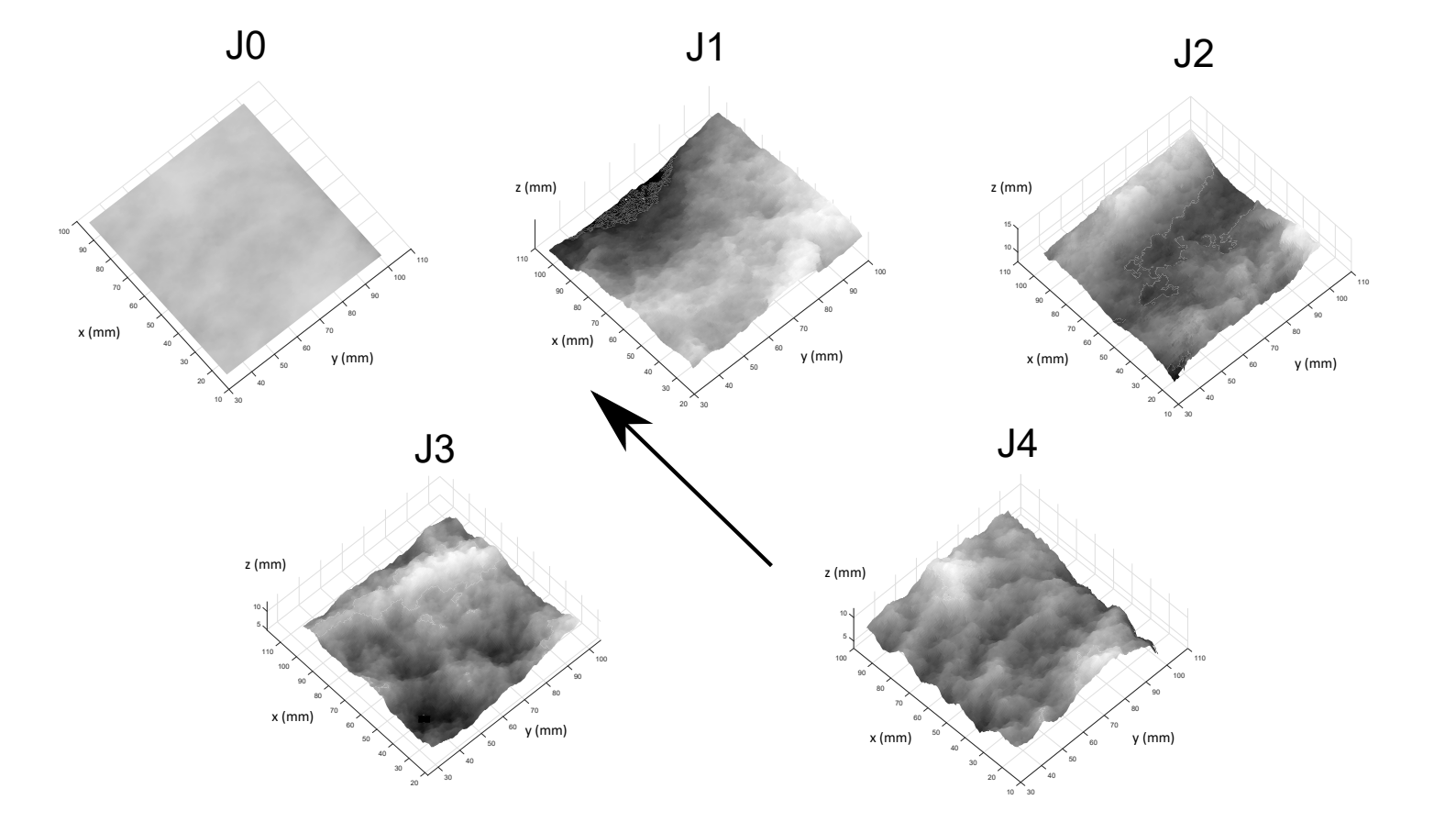
J0
J1
J2
J3
J4
x (mm)
y (mm)
z (mm)

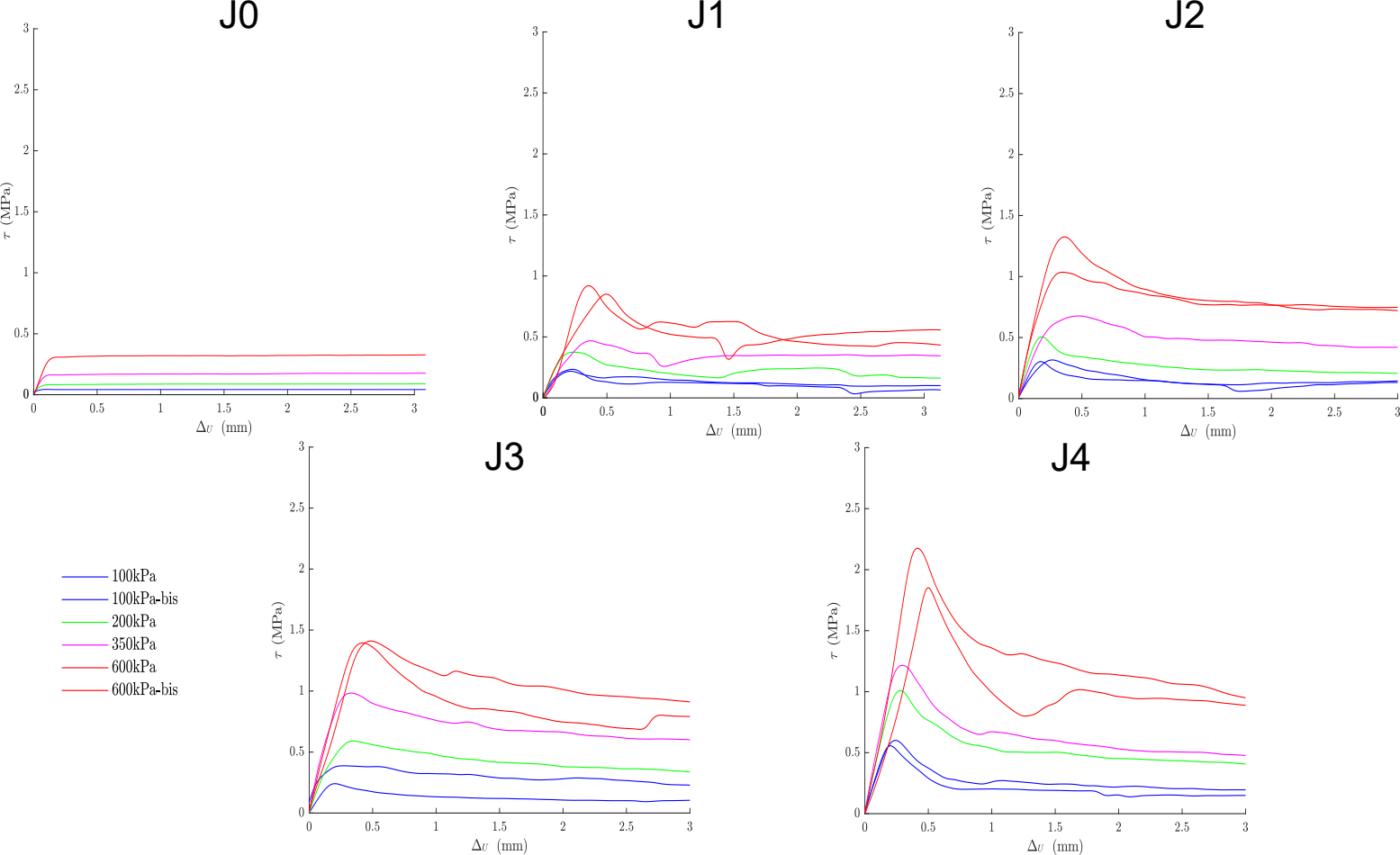
J0
J1
J2
J3
J4
τ (MPa)
Δu (mm)
100kPa
100kPa-bis
200kPa
350kPa
600kPa
600kPa-bis

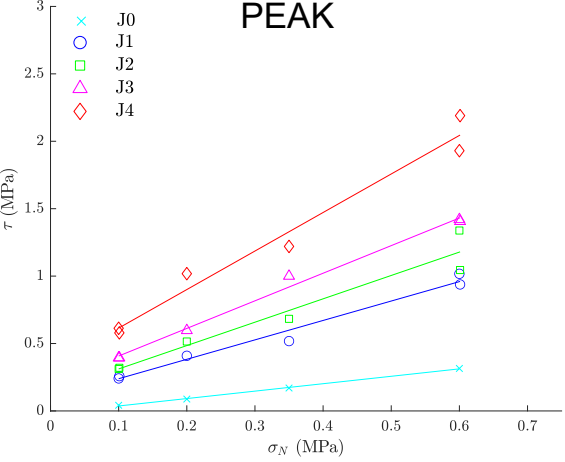
PEAK
J0
J1
J2
J3
J4
τ (MPa)
σN (MPa)
0
0.5
1
1.5
2
2.5
3
0.1
0.2
0.3
0.4
0.5
0.6
0.7

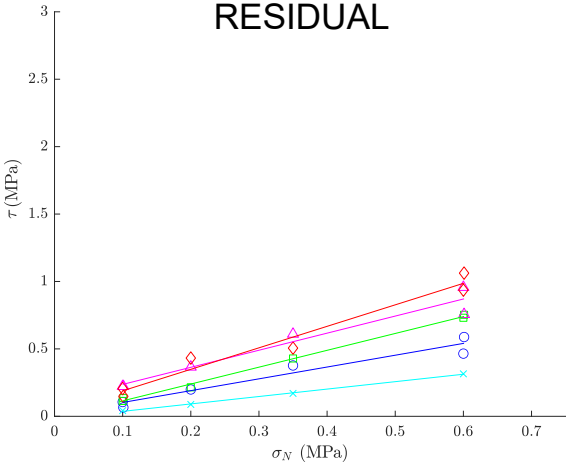
RESIDUAL
τ (MPa)
σN (MPa)
0
0.5
1
1.5
2
2.5
3
0.1
0.2
0.3
0.4
0.5
0.6
0.7

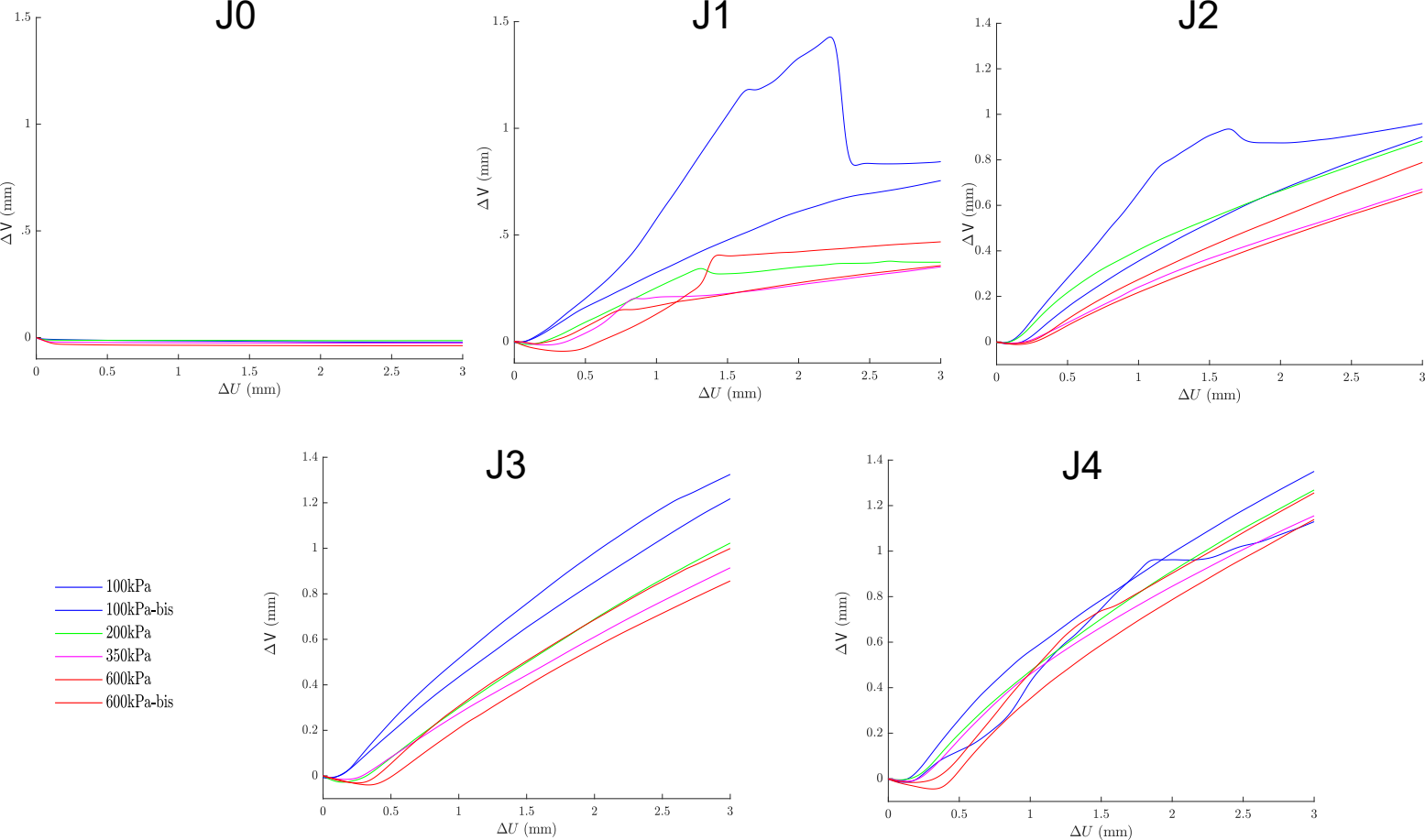
J0
J1
J2
J3
J4
ΔV (mm)
ΔU (mm)
100kPa
100kPa-bis
200kPa
350kPa
600kPa
600kPa-bis

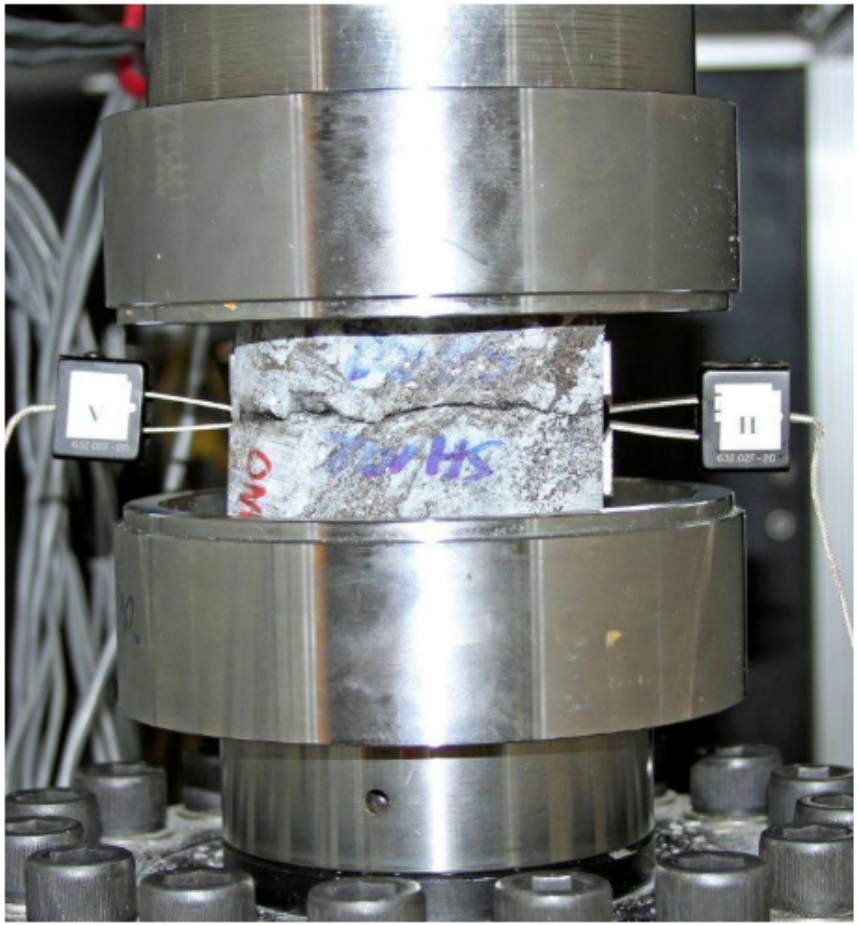

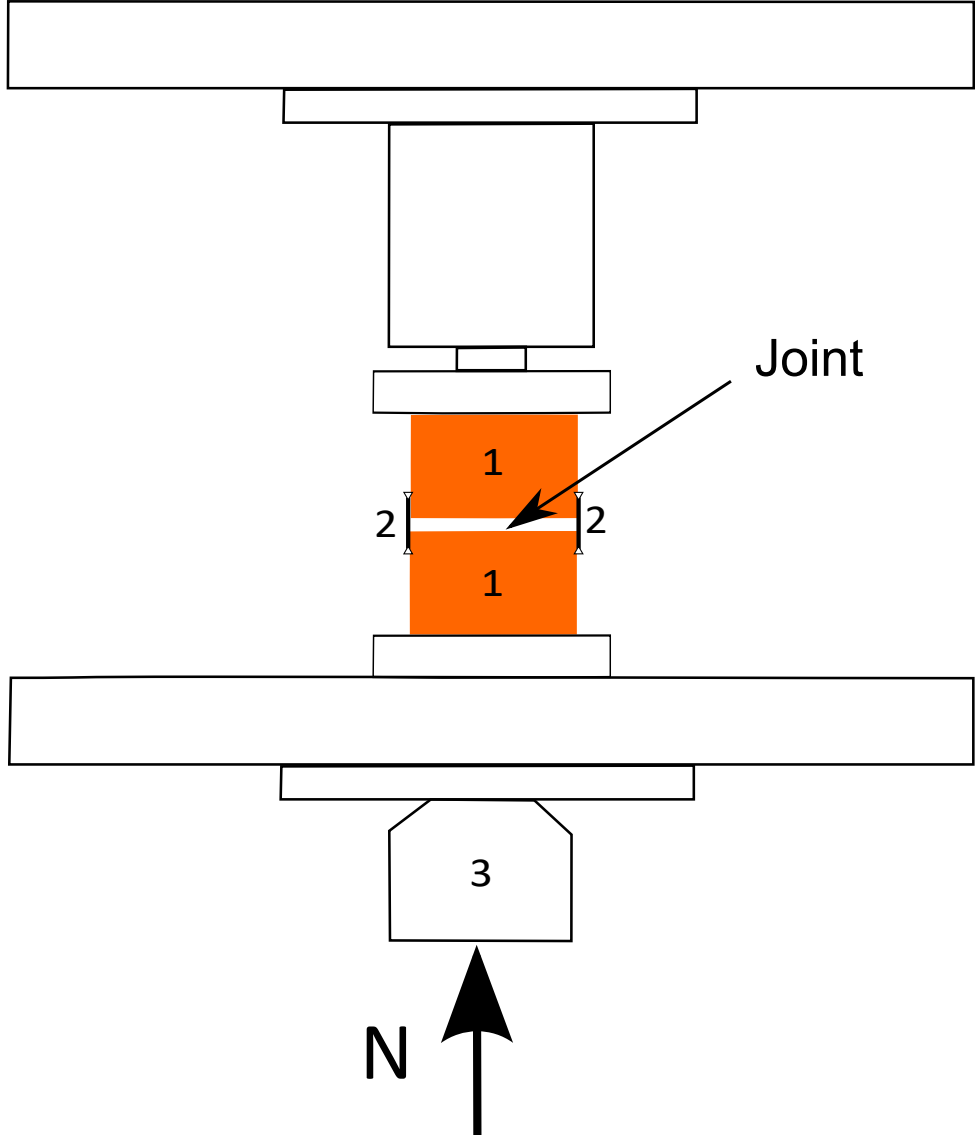
Joint
1
2
2
1
3
N

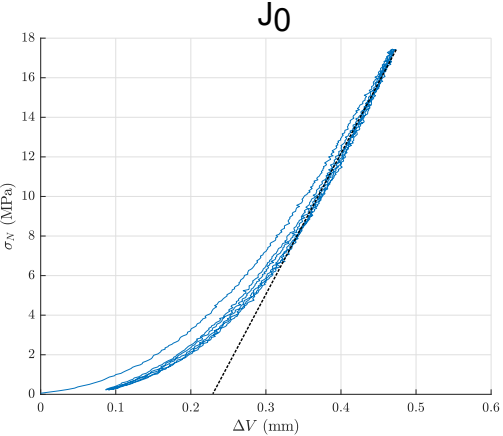
J0
σ_N (MPa)
ΔV (mm)

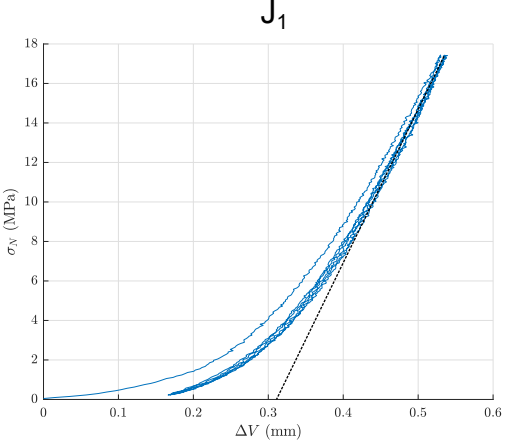
J1
σ_N (MPa)
ΔV (mm)

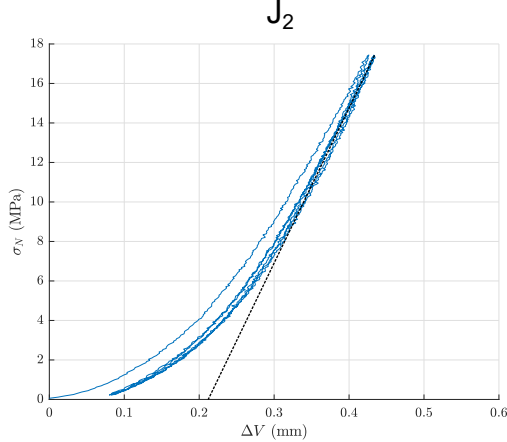
J2
σ_N (MPa)
ΔV (mm)

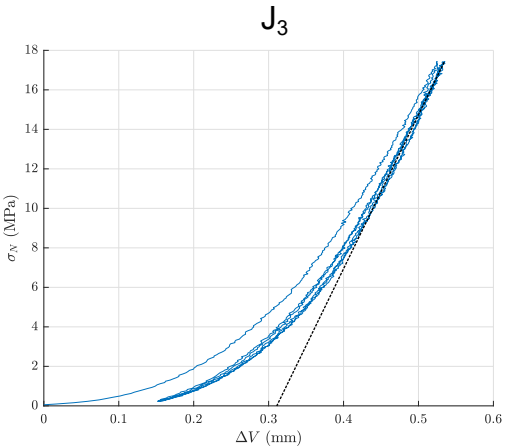
J3
σ_N (MPa)
ΔV (mm)

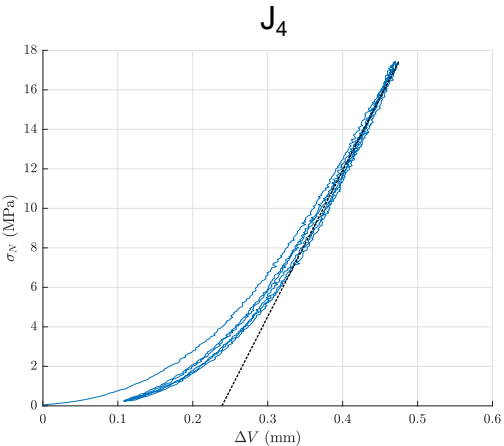
J4
σ_N (MPa)
ΔV (mm)

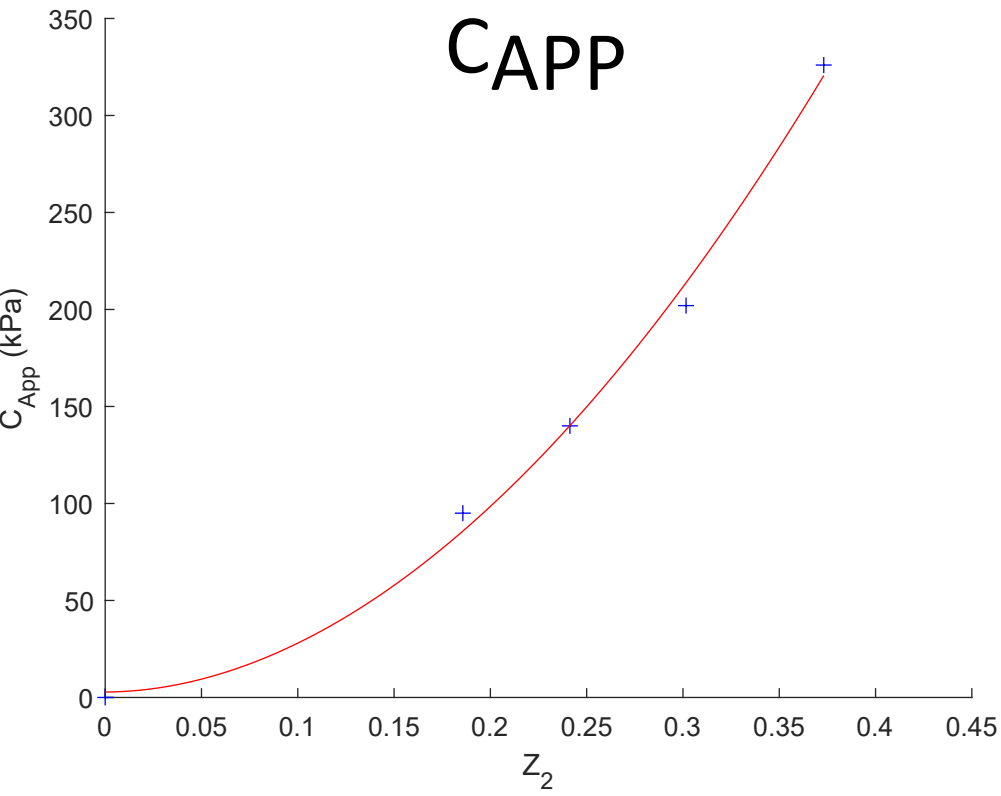

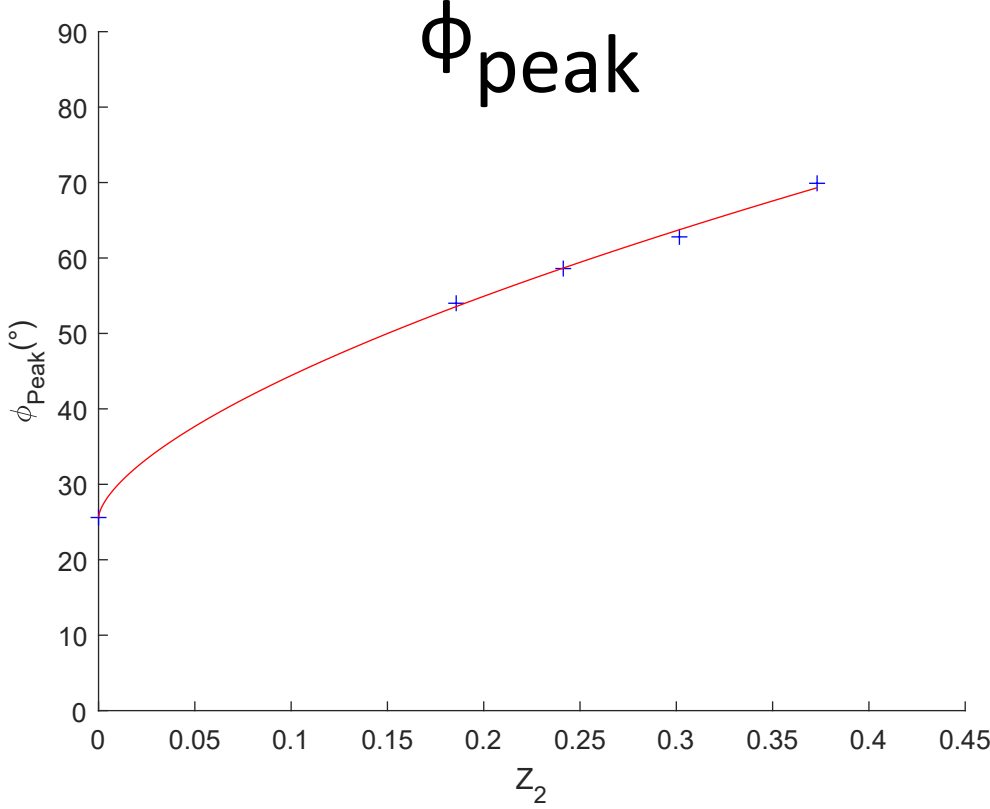

Observed

Estimated

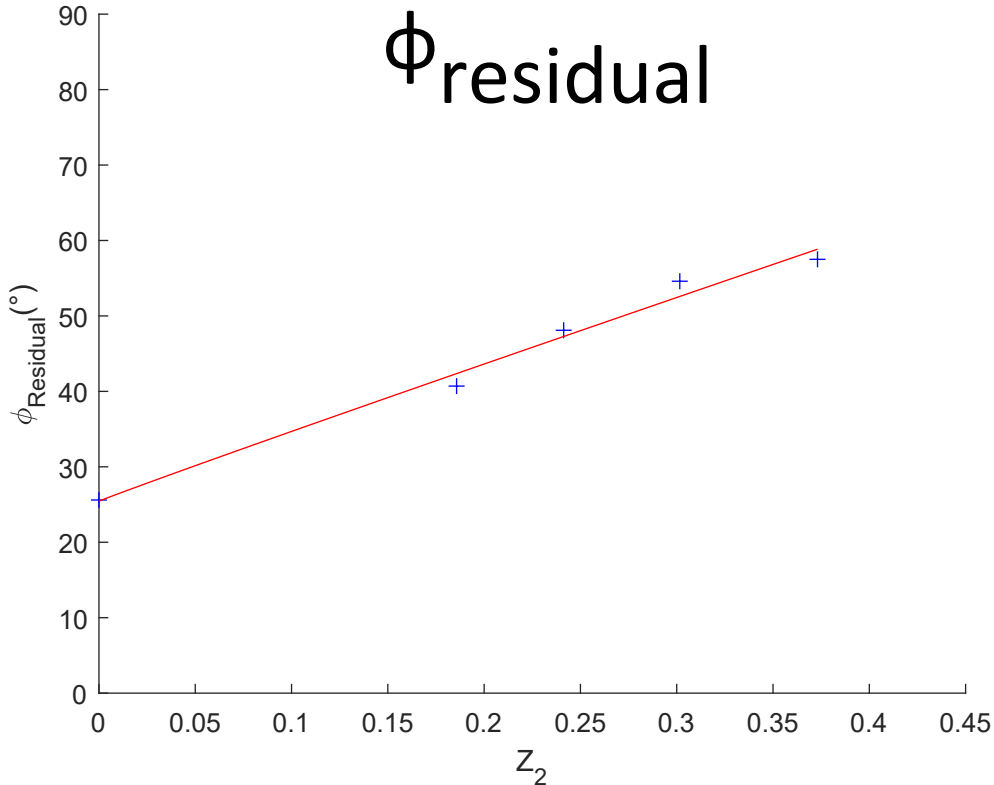

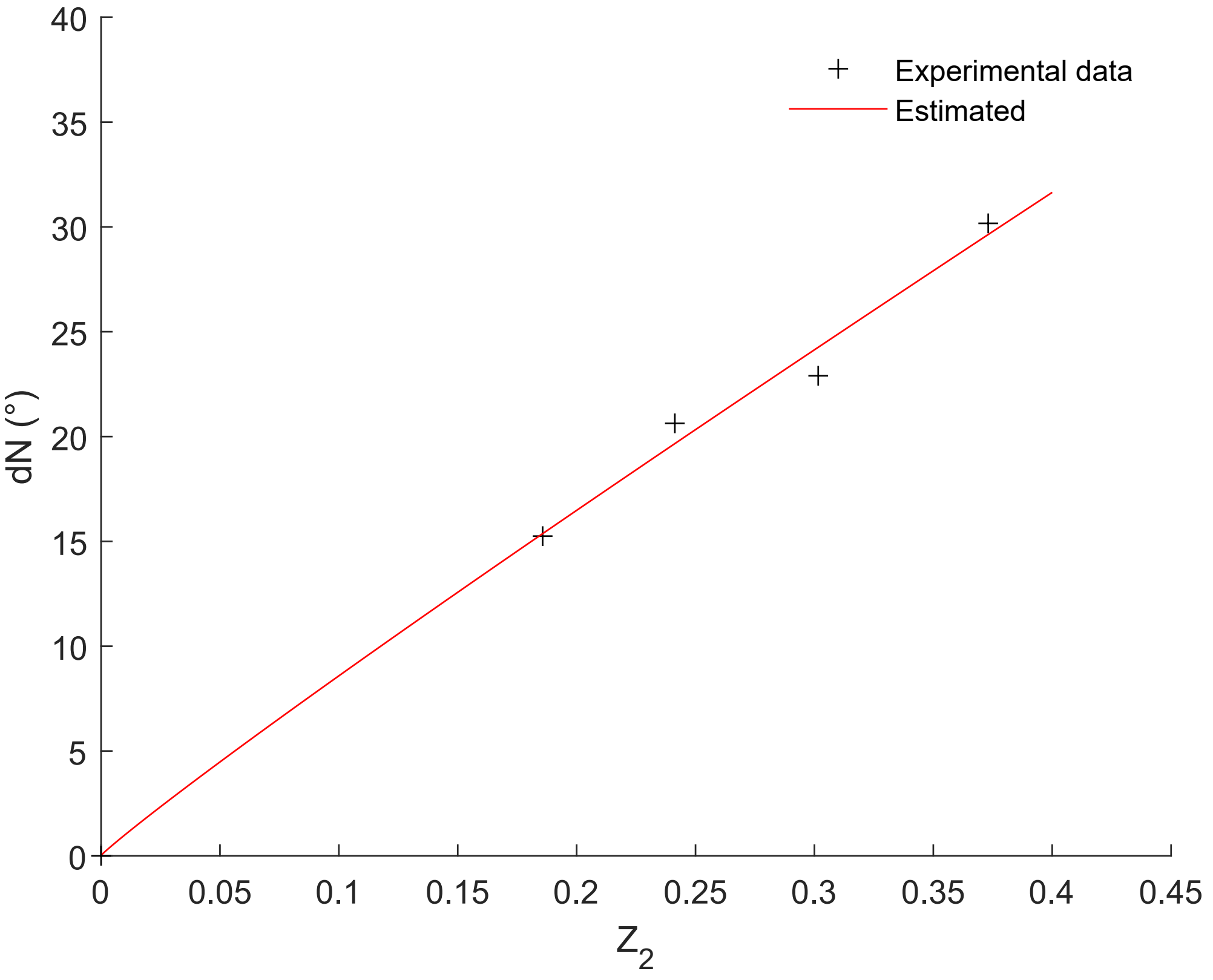
Experimental data
Estimated
dN (°)
Z_2
0
5
10
15
20
25
30
35
40
0
0.05
0.1
0.15
0.2
0.25
0.3
0.35
0.4
0.45

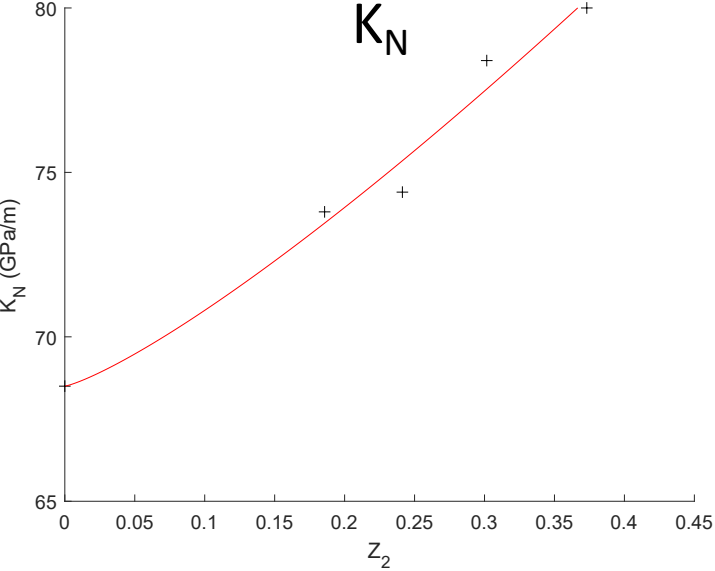

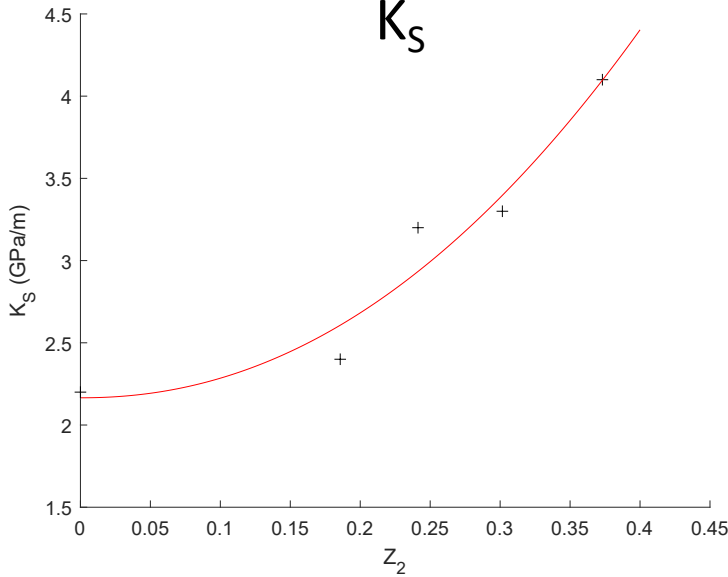

Experimental data

Estimated

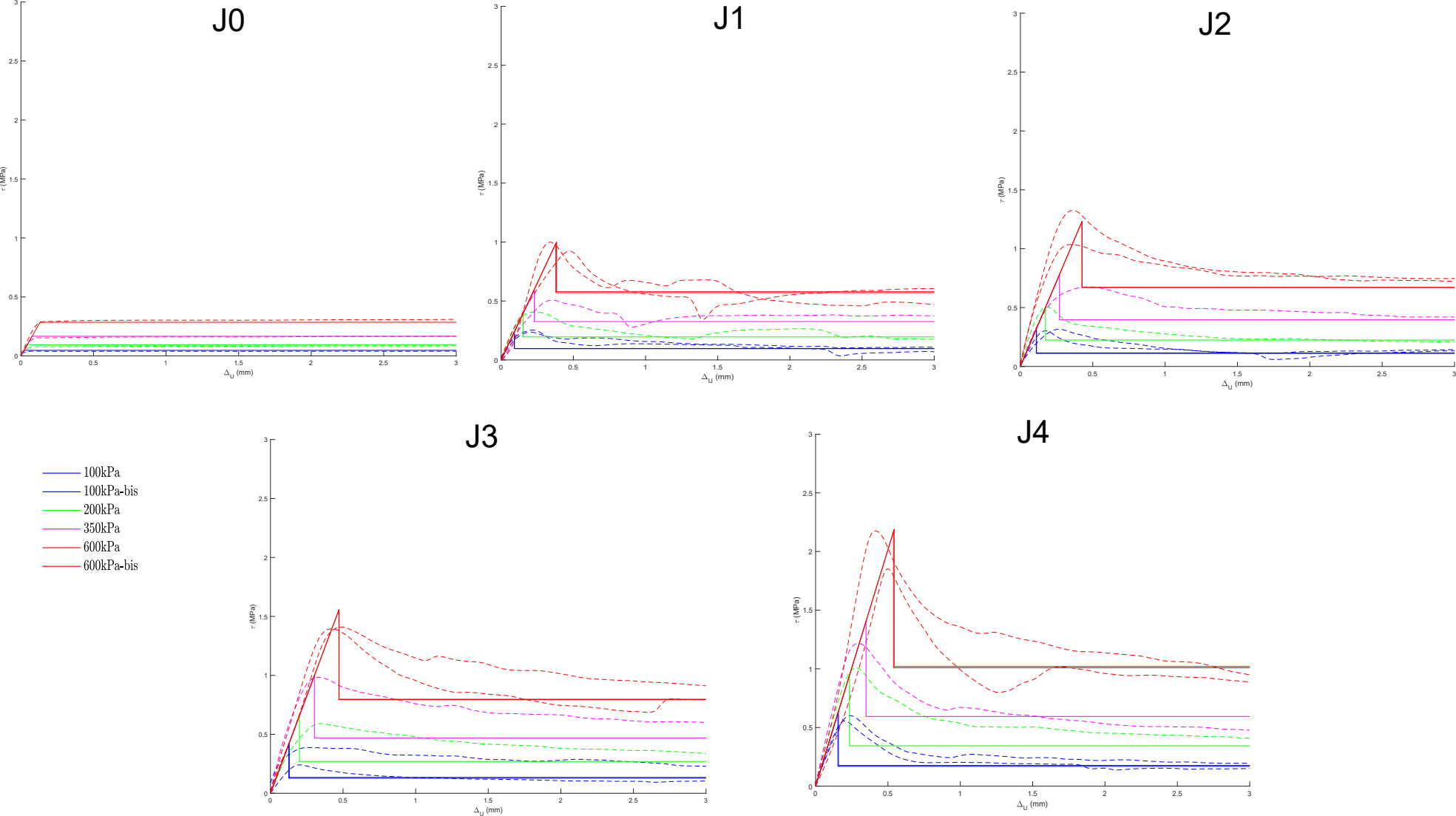
J0
J1
J2
J3
J4
100kPa
100kPa-bis
200kPa
350kPa
600kPa
600kPa-bis
τ (MPa)
Δu (mm)

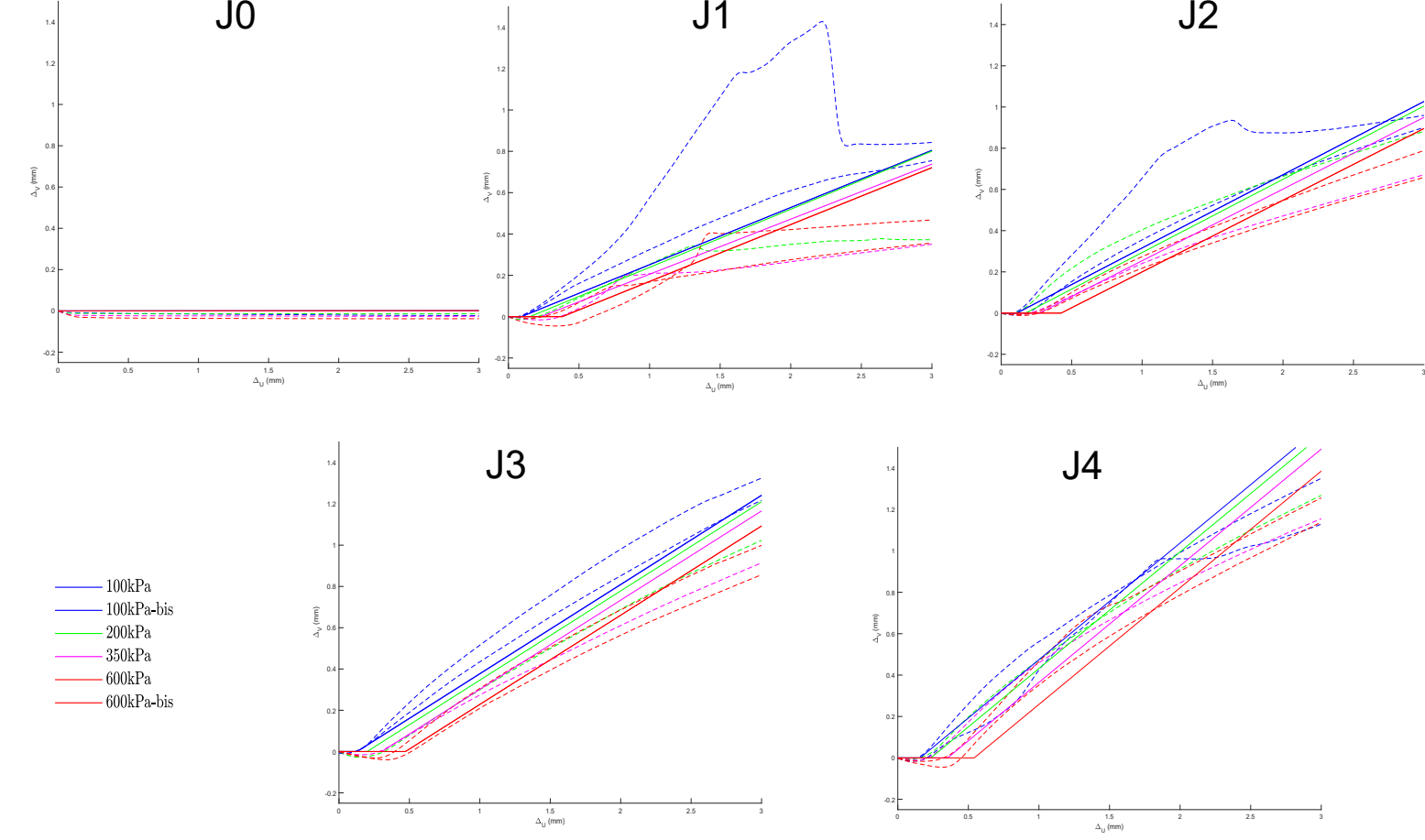
J0
J1
J2
J3
J4
100kPa
100kPa-bis
200kPa
350kPa
600kPa
600kPa-bis
Δ_U (mm)
Δ_V (mm)

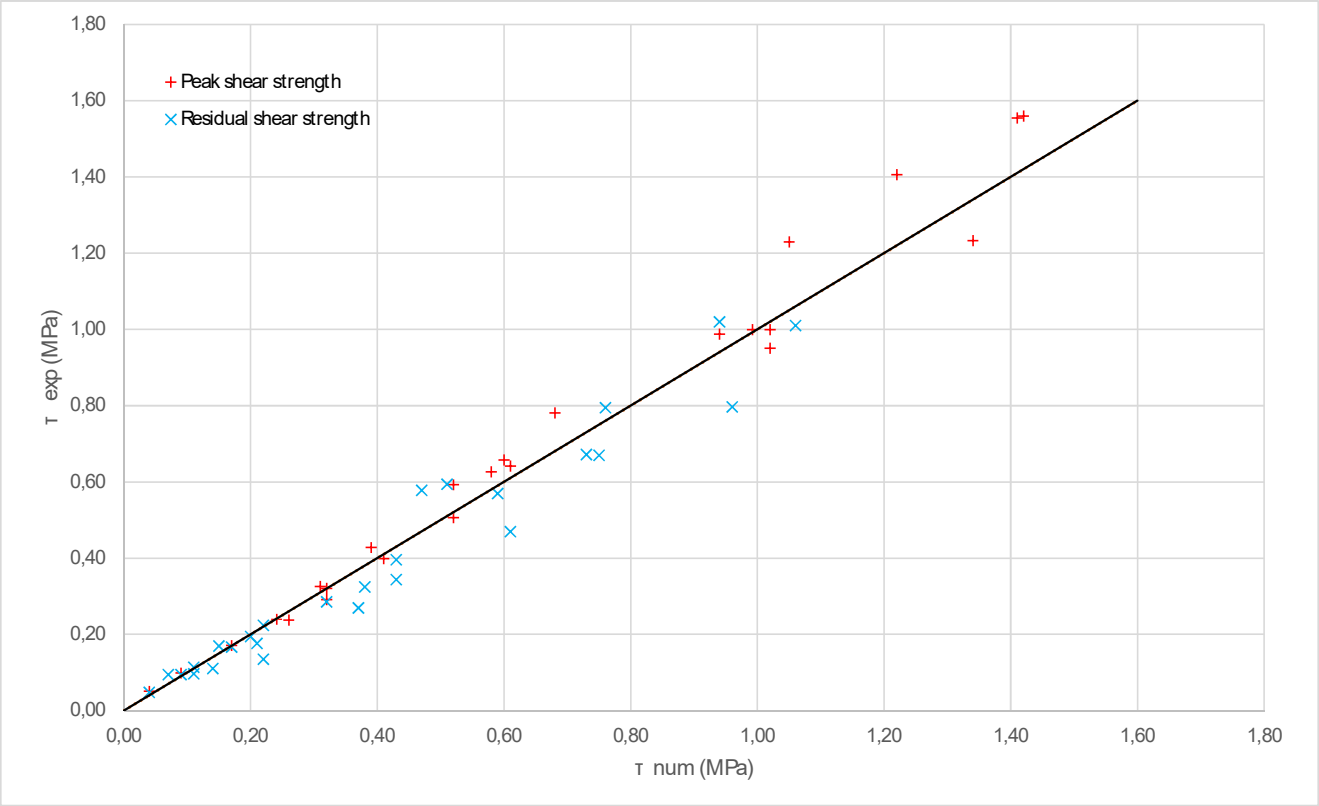
Peak shear strength
Residual shear strength
τ exp (MPa)
τ num (MPa)
0,00
0,20
0,40
0,60
0,80
1,00
1,20
1,40
1,60
1,80

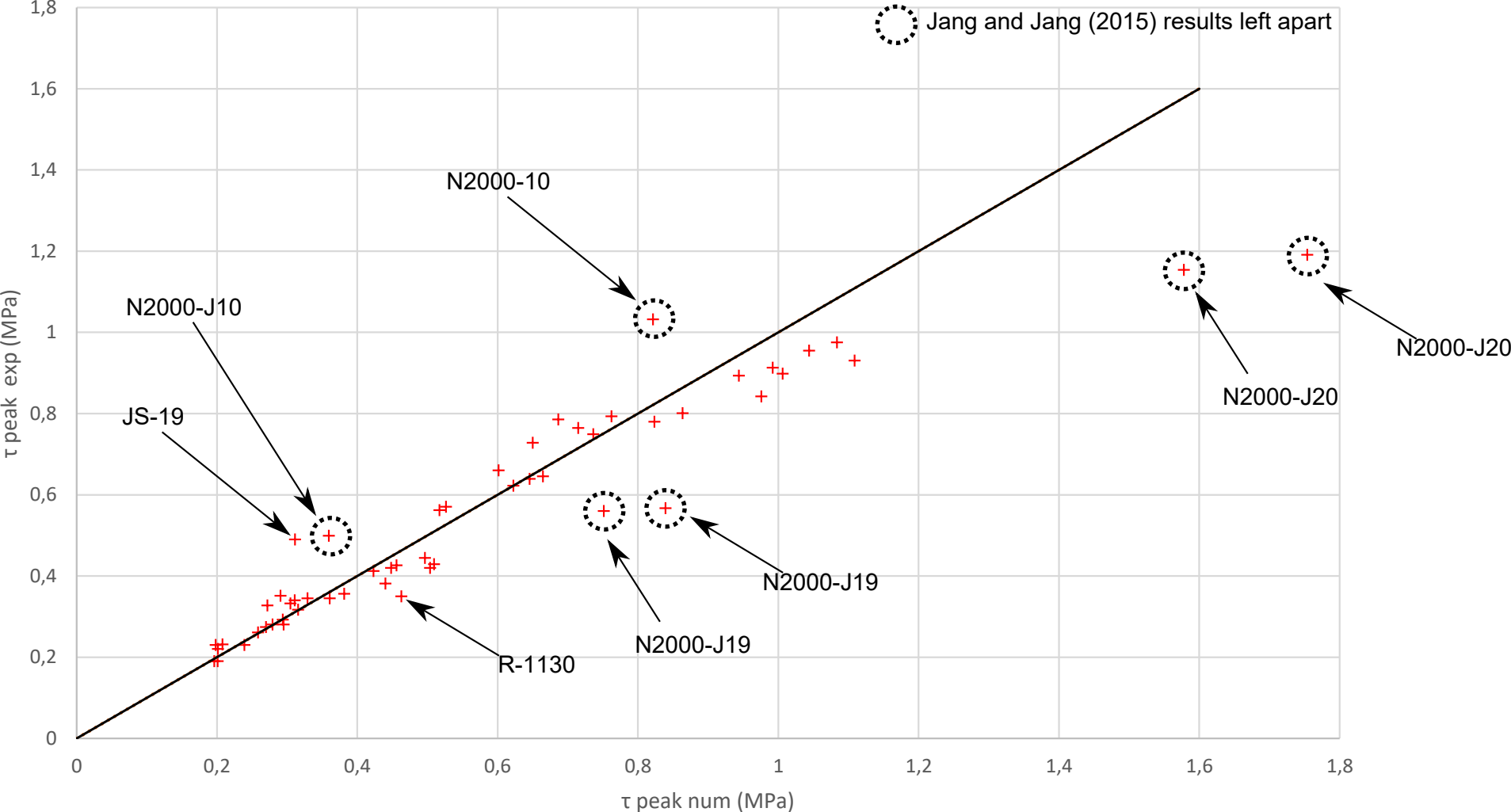
Jang and Jang (2015) results left apart
N2000-10
N2000-J10
JS-19
N2000-J20
N2000-J20
N2000-J19
N2000-J19
R-1130
τ peak exp (MPa)
τ peak num (MPa)
0
0,2
0,4
0,6
0,8
1
1,2
1,4
1,6
1,8

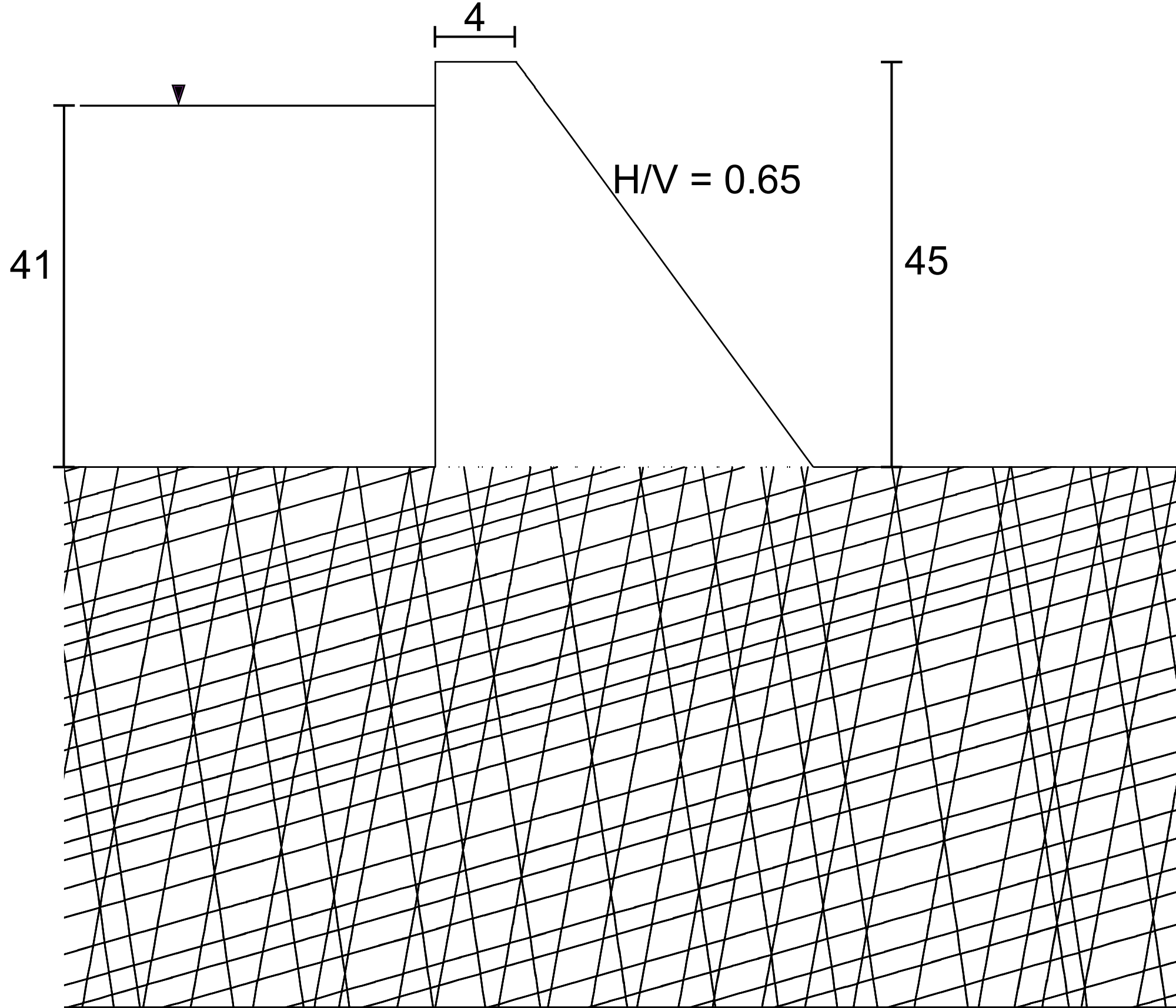
4
H/V = 0.65
41
45

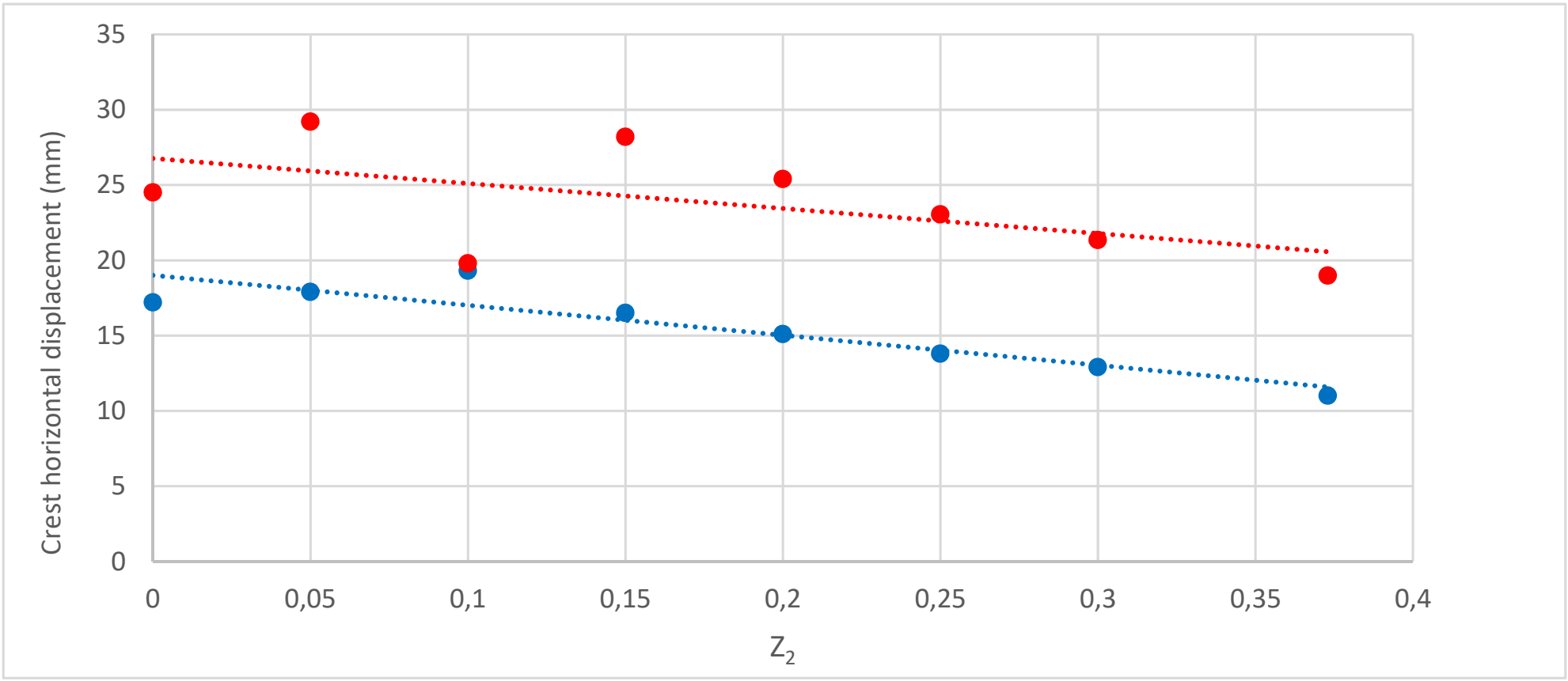
Crest horizontal displacement (mm)
35
30
25
20
15
10
5
0
0
0,05
0,1
0,15
0,2
0,25
0,3
0,35
0,4
Z_2

JOB TITLE :

UDEC (Version 6.00)

LEGEND

3-Sep-2021 11:13:00
cycle 226190
time 6.988E+00 sec

block plot
displacement vectors
maximum = 2.004E-02

2.004E-03	
4.009E-03	
6.013E-03	
8.018E-03	
1.002E-02	
1.203E-02	
1.403E-02	
1.604E-02	
1.804E-02	
2.004E-02	
2.205E-02	

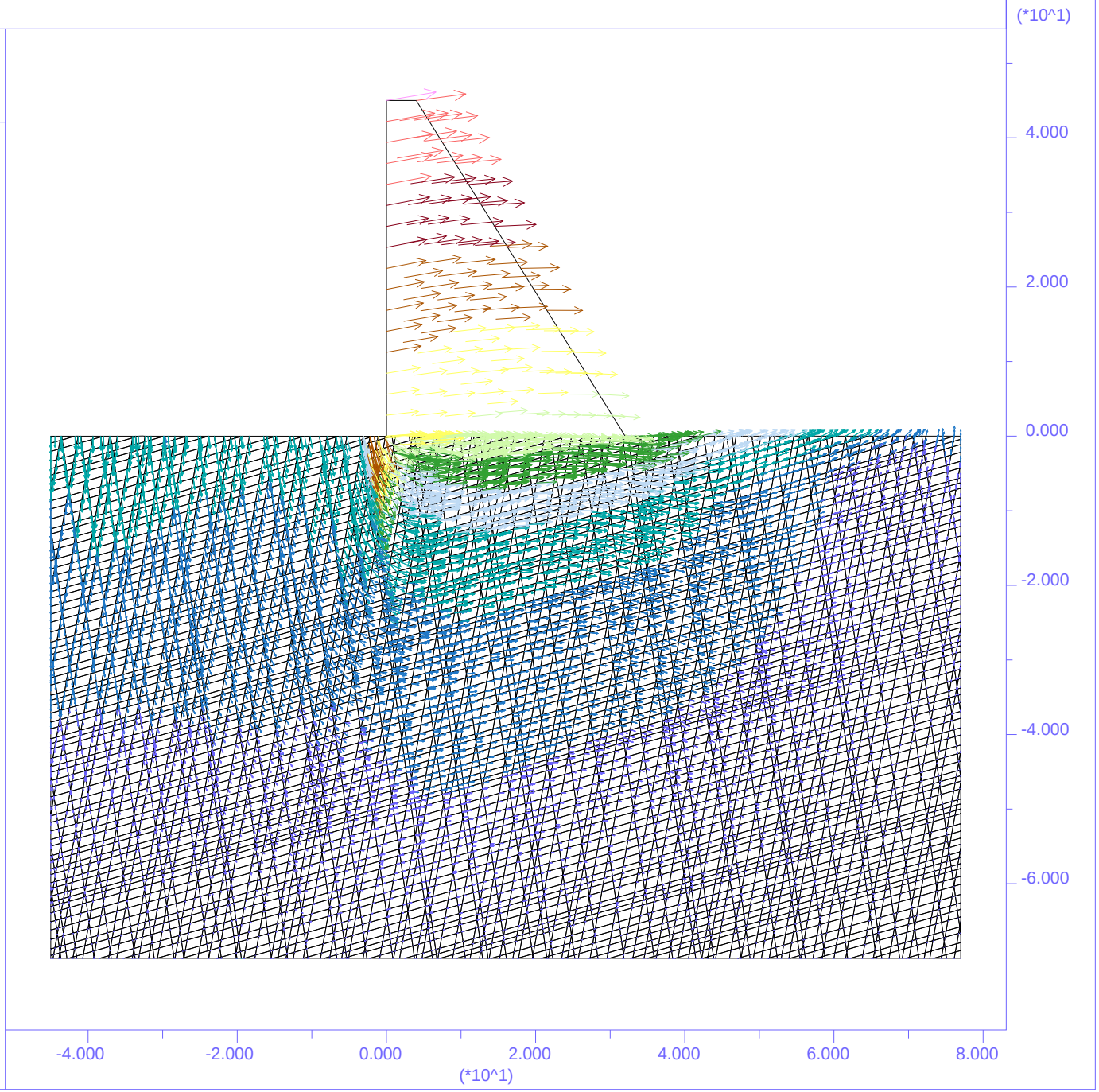

Itasca Consulting Group, Inc.
Minneapolis, Minnesota USA

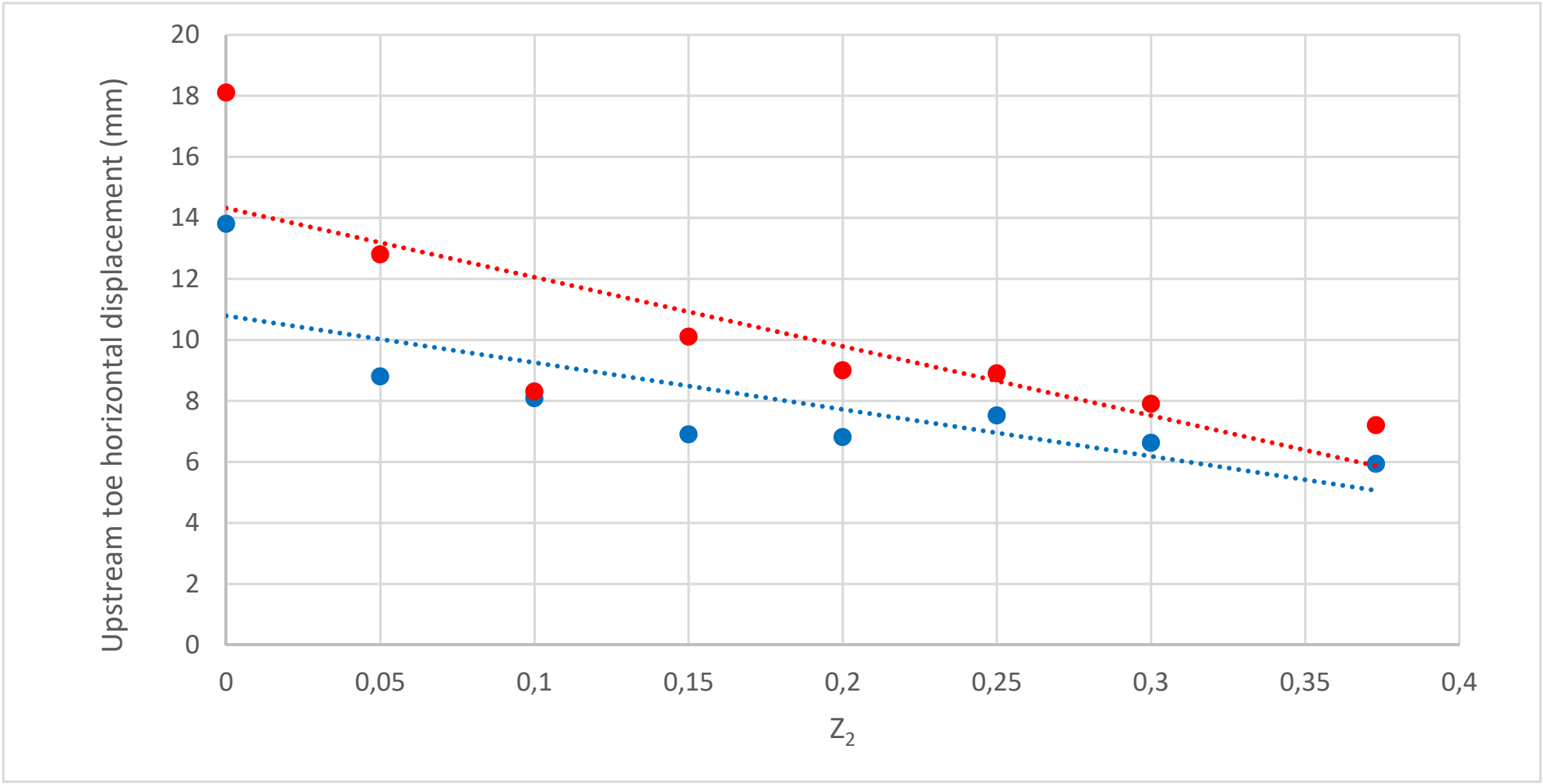
Upstream toe horizontal displacement (mm)
20
18
16
14
12
10
8
6
4
2
0
0
0,05
0,1
0,15
0,2
0,25
0,3
0,35
0,4
Z_2

Integration of rock joint roughness into the Mohr-Coulomb shear behaviour model – Application to dam safety analysis

Adrien RULLIERE [a], Laurent PEYRAS *[a], Jérôme DURIEZ [a], Patrice RIVARD [b] and Pierre BREUL [c]

[a] *INRAE, Aix-Marseille Univ, RECOVER, Aix-en-Provence, France*

[b] *Department of Civil Engineering, Université de Sherbrooke, Sherbrooke, QC, Canada*

[c] *Université Clermont Auvergne, Clermont-Ferrand, France*

* *corresponding author: laurent.peyras@inrae.fr*

ABSTRACT

Based on a previous experimental study that we conducted on granite joint replicas including thirty direct shear tests, this article proposes to integrate the joint roughness in the Mohr-Coulomb shear behaviour model (MC). The model integrates joint roughness into constitutive stress-displacement relationships describing mechanical behaviour of rock joint. The shear strength of rock joint is assessed by the MC shear criterion that takes into account the apparent cohesion. This MC model integrating rock joint roughness component is validated against other experimental results from the literature. It is able to accurately predict the peak shear strength of an unbounded rock joint with an average relative error of 7.9%. It is finally used to assess the role of joint roughness on the shear behaviour of a gravity dam foundation.

KEYWORDS

Apparent cohesion, DEM, Mohr-Coulomb model, rock joint, roughness, shear behaviour

Introduction

The shear strength of unbounded (cohesionless) rock joints have been extensively studied since the 1950s. For such a joint, it is widely accepted that shear strength and behaviour are controlled by many parameters such as joint roughness (Patton 1966; Barton and Choubey 1977; Kulatilake et al. 1995), joint interlocking (Zhao 1997a, 1997b), rock weathering (Barton and Choubey 1977; Nouailletas et al. 2017), joint mechanical properties (Ghazvinian et al. 2010; Rullière et al. 2021) and scale (Bandis et al. 1981; Tatone and Grasselli 2013; Buzzi and Casagrande 2018).

Several failure criteria have been developed to predict joint peak shear strength. The simplest one is the linear Mohr-Coulomb criterion that links the joint peak shear strength (τ_{peak}) to the normal load (σ_N) and joint surface characteristics (C and φ). Barton and Choubey (1977) extended the joint surface characteristic parameter φ of the Mohr-Coulomb criterion to take into account the effects of joint roughness and joint weathering on peak shear strength. Barton-Choubey criterion is well known in rock mechanics (ISRM 2014). This criterion introduces the joint roughness parameter (JRC) determined by visual comparison of the joint with a two-dimensional abacus. Because this abacus cannot cover the wide spectrum of roughness that a joint can exhibit, some authors consider that the JRC value might be prone to subjectivity (Hsiung et al. 1993; Beer, Stead, and Coggan 2002; D. Sow et al. 2016; D. Sow et al. 2017).

Later, Grasselli and Egger (2003) proposed a more complex criterion which adopts a three-dimensional view of the rock joint to estimate its peak shear strength. The criterion proposed by Grasselli and Egger (2003) considers that only the asperities facing the shear direction contribute to joint peak shear strength. Nevertheless, it was demonstrated that this criterion tends to overestimate the peak shear strength of smooth joints ((Xia et al. 2014). More recently, Zhang et al. (2016) proposed a 2D criterion that considers only a proportion of the asperities facing the shear direction. Wang and Lin

(2018) proposed a shear criterion that describes either the sliding or shearing mechanism effects on peak shear strength as a function of the normal stress. Others relevant references in the field of our work have to be cited also (Chen et al. 2022; Wang et al. 2022; Zhang et al. 2022a; Zhan et al 2022b; Barton and Shen 2017; Wang et al. 2020).

Besides assessing the shear strength of joints, it is necessary to evaluate their pre-failure shear behaviour. To this end, several shear behaviour models that analytically describe the interactions between stresses and relative displacements of a joint subjected to shearing have been developed. Historically, the work of Goodman, Taylor, and Brekke (1968) is considered as the first development of numerical laws to model the shear behaviour of rock joints. It suggests that stresses are connected to displacements through mathematical linear elastic laws using constant stiffness, the shear stress being bounded by a maximum value that can be estimated using one of the criteria mentioned above. Later, considerable research improved this model either by considering that stiffness is not systematically constant during shearing (Bandis et al. 1983) or by taking into account the effect of joint damage (Cundall and Lemos 1988). The continuous improvement of computers has led to the development of even more complex and comprehensive shear behaviour models in recent decades. Duriez et al. (2011) developed a shear behaviour model with incrementally non-linear constitutive relations to describe the mechanical behaviour of infilled rock joints along a variety of loading paths. Oh et al. (2015) and Li et al. (2016) proposed a model that considers together and independently the contributions of large-scale roughness (waviness) and small-scale roughness (unevenness) of a joint to its shear behaviour.

For engineering applications such as rock slope stability and dam foundation design, many engineering guidelines suggest using the Mohr-Coulomb criterion to assess the shear strength of a rock joint (USBR 1987; US Army Corps of Engineers 1995; CFBR

2012; ISRM 2014; Federal Energy Regulatory Commission 2016). Mohr-Coulomb input parameters, cohesion C and friction angle φ, are determined through experimental shear tests on small joint samples. For an unbounded rock joint, the cohesion obtained corresponds to the apparent cohesion concept, which depicts the roughness and joint interlocking effect on the shear strength (Amitrano and Schmittbuhl 2002; Rullière et al. 2020). However, guidelines recommend a safe practice considering a low or null value of apparent cohesion, since its extrapolation to the scale of the structure is delicate. But this safe practice is conservative since the resistance characteristics of the joint due to its morphology (roughness, interlocking) are neglected.

The aim of this article is to integrate rock joint roughness components into the Mohr-Coulomb shear behaviour model which is chosen for its wide usage in engineering practice strength (USBR 1987; US Army Corps of Engineers 1995; CFBR 2012; ISRM 2014; Federal Energy Regulatory Commission 2016), in order to take into account the role of joint roughness on joint shear behaviour. This integration aims to take into account the role of joint roughness on joint shear behaviour and is built up on the base of thirty-five experimental tests (direct joint shear tests and joint compression tests) and links joint roughness to joint shear behaviour and strength. The rock joint shear behaviour is described through stress-displacement laws. Joint failure state is expressed by the Mohr-Coulomb criterion including the apparent cohesion concept, to stick to the current practice of rock engineering. At the end, the MC shear behaviour model integrating rock joint roughness is validated with experimental data coming from rock mechanics literature.

The paper is divided into four parts. The first part presents the materials and methods (Part 1). In the second part, the MC shear behaviour model integrating rock joint roughness is developed and calibrated (Part 2). It consists in the development of empirical laws correlating the joint roughness to the shear behaviour model input parameters. These

empirical laws are then integrated in the MC model, so that it takes into account the role of joint roughness on joint shear behaviour. In the third part, the developed model is validated in the third part: model blind-predictions are faced to direct shear test results from rock mechanics literature in order to evaluate the model's accuracy (Part 3). In the last part, the MC shear behaviour model integrating rock joint roughness is used to demonstrate the key role of joint roughness on the shear behaviour of a gravity dam foundation (Part 4). All the numerical calculations presented in this paper were performed using the Discrete Element Method (DEM).

1. Materials and Methods

This part presents: i) the experimental data used to develop the empirical equations linking the joint roughness to the shear behaviour model input parameters, ii) the shear behaviour model used in the study, and iii) the DEM code in which the model will be implemented to predict the shear behaviour at the laboratory and gravity dam scales.

1.1.Experimental data used to develop the shear behaviour model

The experimental data come from a previous work (Rullière et al. 2020) and are summarized in this article. Thirty direct shear tests on granite joint replicas were carried out in CNL conditions and under 0.1, 0.2, 0.35 and 0.6 MPa normal stress. Additional joint compression tests were conducted to characterize the joint normal stiffness. The tests were specifically performed for the research work presented in this paper.

It is specified in this introduction to the experimental data that our work does not take into account the scale effect between the sample tested in the laboratory and the real scale model. Several authors such as (Bandis et al. 1981) have worked on the scale effect and have shown the influence of sample size on shear strength. This question of scale

126 effect between laboratory and field is, in general, a universal problem of this kind of study
127 that our research has not taken into account.

128 *1.1.1. Joint roughness statistical indicator (Z_2)*

129 Many studies have been conducted to define the roughness concept because it is
130 considered to be the main parameter governing the shear behavior of rock discontinuities.
131 Barton and Choubey (1977) developed the joint roughness coefficient (JRC) to estimate
132 joint roughness using a visual comparison of 10 standard profiles. With the advancement
133 of non-contact methodologies used to scan rock joint surfaces, new parameters have been
134 developed to assess roughness. In this context, the 2D directional parameter Z_2 is widely
135 accepted and used in the rock mechanics community as a non-subjective roughness
136 indicator (Tse and Cruden 1979; Kulatilake et al. 1995; Tatone and Grasselli 2010;
137 Magsipoc, Zhao, and Grasselli 2019; Ram and Basu 2019). Indeed, for a joint profile, the
138 parameter Z_2 is a 2D directional parameters that describes the local topographic slope of
139 the joint profile. Z_2 can be seen as a topographical slope and corresponds to the root-
140 mean-square of the first derivative (Myers 1962). Z_2 can be calculated as:

141 $$Z_2 = \left[\frac{1}{L}\sum_{1}^{n-1}\left(\frac{y_{i+1}-y_i}{x_{i+1}-x_i}\right)^2\right]^{\frac{1}{2}} \quad (1)$$

142 Where L is the length of the joint profile, x_i and y_i are the coordinates of the
143 discretized joint profile (0.5 mm sampling interval).

144 The calculation of Z_2 requires only a topographic scan of the joint surface and, in
145 comparison to other roughness indicators, it is rather simple and non-time-consuming to
146 implement the calculation of Z_2 in an algorithm.

147 Five granite joints (J0, J1, J2, J3, J4) with different roughness's (Z_2 from 0 to
148 0.373) were selected to produce the replicas. Prior to replica production, the granite joints
149 were scanned with a non-contact laser profilometer (Figure 1). Data from the scans were

150 then implemented in a specifically designed algorithm linking the surface morphology to
151 the roughness statistical parameter Z_2 (Rullière et al. 2020). Table 1 shows the Z_2 value
152 for each of the five granite joints used to produce the replicas.

153 [FIGURE 1 HERE]

154 [TABLE 1 HERE]

155 *1.1.2. Direct shear test*

156 Following the production of the replica (six replicas per selected roughness), thirty direct
157 shear tests were conducted in CNL conditions. Twenty direct shear test results, carried
158 out on J0, J1, J2, J3 and J4 under 0.1, 0.2, 0.35 and 0.6-MPa normal stress come from the
159 results of Rullière et al. (2020). For this work, ten additional direct shear tests were carried
160 out for J0, J1, J2, J3 and J4, under 0.1 and 0.6-MPa. These new results provide more shear
161 tests results over the 0.1 to 0.6-MPa interval and strengthen the Mohr-Coulomb failure
162 envelope plot. The normal stress levels used in this study correspond to those observed
163 in dam foundations or other civil engineering works (Sow et al. 2017). Each replica was
164 used for a single direct shear test.

165 Figure 2 shows the shear strength versus shear displacement curves for all the
166 direct shear tests used in this study. The key data are summarized in Table 2. It classically
167 appears from the direct shear tests results that the rougher the joint, the higher the shear
168 strength (peak or residual).

169 [FIGURE 2 HERE]

170 [TABLE 2 HERE]

171 Figure 3 depicts the Mohr-Coulomb failure envelopes plotted from the
172 experimental direct shear test results for the peak and residual shear strengths. Apparent
173 cohesion and friction angle values at both peak and residual stages are shown in Table 1.
174 Again, it appears that the rougher the joint, the higher the apparent cohesion and friction

angle values. Since the results were obtained on an unbounded rock joint replica, it was considered that the apparent cohesion could be mobilized at peak stage only (EPRI 1990; Rullière et al. 2020). Therefore, $C_{APP\ Residual}$ = 0-kPa.

[FIGURE 3 HERE]

The shear stiffness K_S was calculated for shear stresses ranging from 25 to 75% of the peak shear strength (Kumar and Verma 2016). This precaution allows setting aside the curved areas of the shear strength-shear displacement curve (initial loading and peak phase). Table 1 presents the K_S mean value obtained for all the joints tested. It appears that the rougher the joint, the higher the shear stiffness.

Figure 4 shows normal versus shear displacement curves for all the direct shear tests (Rullière et al. 2020). It is verified that the dilatant behaviour depends on both of the joint roughness and the normal stress imposed during the shear tests. As shown in Figure 4, a rougher joint lead to larger normal displacement during a direct shear test in CNL conditions. The dilatancy angle (dN) is calibrated from the maximal value of the Δ_V / Δ_U ratio (usually around the peak shear displacement value). Table 1 shows the dN mean value obtained for all the joints tested. As expected, the rougher the joint, the higher the dilatancy angle.

[FIGURE 4 HERE]

1.1.3. Compression test results

Joint normal stiffness (K_N) assessment requires specific experimental tests called joint compression test (Bandis et al. 1981; Fan, Cao, and Tang 2018). Such a test involves recording the relative normal displacements of a rock joint under a given normal load (Figure 5).

[FIGURE 5 HERE]

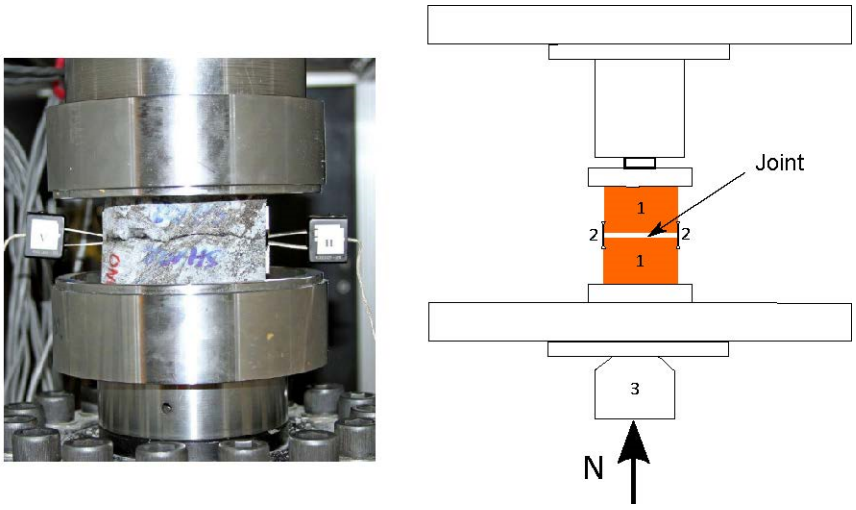

In practice, several loading-unloading cycles are performed to determine the normal stiffness of a rock joint (Bandis et al. 1983; Marache 2002). The first cycle allows the joint to be fully interlocked, so that the deformations recorded during the following cycles correspond to the joint's deformations only and not to a change of joint interlocking.

Five joint compression tests were performed, for each granite joint. The joints were subjected to an increasing normal stress, up to 30% of the compressive strength matrix of the material, prior to a progressive discharge. The charge-discharge cycles were repeated three times and the K_N was measured along the last loading cycle. Figure 6 shows the normal stress versus normal displacement curves obtained from the joint compression tests. The K_N value of each joint is presented in Table 1. If the K_N values are compared to joint roughness, it seems that the rougher a joint, the higher the K_N.

[FIGURE 6 HERE]

1.2. Shear behaviour model used in the study

The shear behaviour model used in this study follows an elastic-plastic formulation based on the work of Goodman, Taylor, and Brekke (1968). As a joint is subjected to a shear stress, the response of the joint is initially exclusively elastic. The displacements can be

correlated to the normal or shear stress variations through constant joint normal or shear stiffness and classical linear elastic laws:

$$\begin{pmatrix} \mathrm{d}\sigma_N \\ \mathrm{d}\tau \end{pmatrix} = \begin{pmatrix} K_N & 0 \\ 0 & K_S \end{pmatrix} \cdot \begin{pmatrix} d\Delta_V \\ d\Delta_U \end{pmatrix} \quad (2)$$

Where $d\sigma_N$ is the normal stress variations, $d\tau$ is the shear stress variation, K_N is the joint normal stiffness, K_S is the joint shear stiffness, $d\Delta_U$ is the shear displacement increment and $d\Delta_V$ is the normal displacement increment.

A direct shear test conducted in Constant Normal Load (CNL) conditions is piloted by constant tangential displacement increments ($d\Delta_U$). Therefore, the shear stress progressively increases according to (2). On the contrary, the normal stress increment is null. In this type of test, this means that the model assumes no normal displacement increments ($d\Delta_V$) during the elastic stage.

The elastic stage extends until the shear stress τ reaches the shear strength value τ_{peak} defined by the Mohr-Coulomb criterion which serves as both a (constant) yield surface and plastic limit condition in the $(\tau;\sigma_N)$ plane, in the absence of elasto-plastic hardening. As rock joints are unbounded, the cohesion of the Mohr-Coulomb criterion corresponds to the apparent cohesion, C_{app}, as presented in the introduction.

$$\tau = C_{app} + \sigma_N.\tan(\varphi) \quad (3)$$

Where τ is the shear stress, σ_N is the normal stress, C_{app} is the apparent cohesion and φ is the friction angle.

As soon as the peak shear stress is reached, the shear behaviour model considers that the joint is in a failure phase: the elastic stage is completed and the plastic stage begins. The shear stress decreases instantaneously to the residual and constant value $\tau_{residual}$. This choice of a brittle behaviour, as opposed to a gradual softening, is chosen for simplicity, in line with engineering practices.

In the plastic stage, a flow rule governs the dilatancy whereby normal displacement variations are correlated to shear displacement variations and to the joint dilatancy angle:

$$d\Delta_V = d\Delta_U.\tan(dN) \quad (4)$$

Where $d\Delta_U$ is the shear displacement increment, $d\Delta_V$ is the normal displacement increment and dN the dilatancy angle.

1.3.The Discrete Element Method

A rock mass can be considered as a set of rocky blocks separated from each other by joints. For such a set, a mechanical stress will lead to displacements that are almost exclusively due to the displacements along the joints (the rocky block deformations are considered as insignificant). This consideration exactly matches the DEM hypothesis: blocks are considered as infinitely stiff and the displacements are exclusively due to block contacts.

The DEM method and UDEC software (Itasca 2019) were used in this paper to perform the different numerical calculations, either to simulate laboratory direct shear tests in CNL conditions or to assess the shear behaviour of a gravity dam founded on a complex jointed rock mass. In UDEC, the hydro-mechanical behaviour of a set of blocks and joints is simulated by adjusting the joint properties (mechanical properties and behaviour models).

2. Calibration of the MC shear behaviour model integrating rock joint roughness

2.1. Equations linking joint roughness to shear behaviour model input parameters

The aim of this section is to develop empirical equations that correlate the joint roughness to the input parameters of the MC shear behaviour model integrating rock joint roughness. These input parameters are $C_{app\ peak}$, φ_{peak}, $C_{app\ residual}$, $\varphi_{residual}$, dN, K_N and Ks (see section 1 for more details). The experimental data presented in Part 1 are used and three kinds of mathematical laws are studied: linear, power, and exponential laws. For each kind of law, the least square method was used to determine coefficients *a*, *b* and *c* :

$$P = a \,.\, Z_2 + b \tag{5}$$

$$P = a \,.\, Z_2^{\,b} + c \tag{6}$$

$$P = a \,.\, e^{Z_2 . x} + c \tag{7}$$

Where *a*, *b* and *c* are empirical coefficients and P stands for any model parameters among $C_{app\ peak}$, φ_{peak}, $C_{app\ residual}$, $\varphi_{residual}$, dN, K_N and K_S.

For the sake of concision, only the power equations are presented. Indeed, it appeared during the study that the power equations (6) were able to correlate the joint roughness to the shear behaviour input parameter with great precision. In comparison to linear and exponential equations, the power equations had the highest coefficient of determination (R^2). However, the reader will find linear and exponential equations in Appendix A.

Based on the data presented in Table 1, the power law equations describing the shear behaviour and shear failure state of the joint are developed. Power law coefficients

a, *b* and *c*, which correlate the roughness to the peak apparent cohesion, peak friction angle, residual friction angle, dilatancy angle, and normal and shear stiffness, are presented in Table 3. Figures 7 to 9 compare the power law predictions to the experimental data.

The values of coefficients *a, b* and *c* and the equations developed in this section are valid only for the following conditions:

- the rock joint roughness is described by the Z_2 statistical parameter. Z_2 ranges between 0 (smooth joint) and 0.373 (rough joint);
- the rock joint is subjected to a normal load ranging from 0.1 to 0.6-MPa.

[TABLE 3 HERE]

[FIGURE 7 HERE]

[FIGURE 8 HERE]

[FIGURE 9 HERE]

2.2.*Numerical direct shear tests using the MC shear behaviour model*

Once the shear behaviour model was established, thirteen numerical direct shear tests were performed under the exact same conditions of normal load and roughness as the experimental direct shear tests presented in the previous section. In other words, data provided by the numerical shear behaviour model were compared to the experimental data used to develop it, to control if the numerical results fit the experimental observations and if the calibration of the numerical model had been carried out well.

Using UDEC software (Itasca 2019), the rock joint is represented by the contact between two infinitely rigid blocks. While the lower block is fixed, the upper block is subjected to both a normal load and a constant horizontal displacement rate. In the DEM model, the lower block length is longer than the upper block to avoid any toppling of the

upper block. For the numerical direct shear tests, the normal load and horizontal displacement rate were set as equal to the experimental values applied during the experimental direct shear tests (normal load ranges from 0.1 to 0.6-MPa and the horizontal displacement rate is 0.1 mm/min to insure quasi-staticity). The numerical model also required the roughness of the joint (depicted by Z_2).

Figure 10 and Figure 11 show the shear stress versus horizontal displacement curves and normal displacement versus horizontal displacement curves. The dotted lines correspond to the experimental data, while the full lines correspond to the numerical results.

From Figures 10 and 11, it appears that despite its bilinear aspect, the numerical model manages to describe the rock joint shear behaviour efficiently. This is particularly true during the peak phase, and to a lesser extent for the residual phase (end of test). Nonetheless, as shown in Figure 10, the post-peak joint behaviour is not realistically described by the shear behaviour model since as soon as the peak shear strength is reached, the release of the shear stress is instantaneous, while the experimental tests show a progressive decrease of the shear stress towards a residual shear stress value. Figure 11 shows that the shear behaviour model satisfactorily reproduces the dilatant behaviour of a rock joint, although there is no contraction stage and for the shear behaviour model, the dilatancy starts as soon as the shear stress reaches its peak (these are related to the equations that govern the MC shear behaviour model, see Part 1). However, it should be noted that in rock-mechanics engineering practice, the post-peak shear behaviour has not been extensively studied and the MC model approximations could be sufficient for a vast majority of applications.

Figure 12 displays the model peak and residual shear strength and contrasts it with the experimental recorded values. For the peak stage, the results predicted by the model

333 are very close to the experimentally recorded values (generally, the difference is less than
334 10%). For the residual phase, the differences are slightly larger, but can be explained by
335 the numerous jumps present on the experimental curves (Figure 2).
336
337 [FIGURE 10 HERE]
338 [FIGURE 11 HERE]
339 [FIGURE 12 HERE]
340 The shear behaviour model can be considered as calibrated, as the numerical shear
341 test results matches the experimental results.
342 The next step consists of a validation in which we aim to assess the ability of the
343 shear behaviour model to predict the rock joint shear behaviour of all rock joints. To this
344 end, the aim of the next section is to compare the model blind-predictions to other
345 published experimental direct shear test results that were not used to develop the
346 numerical model.

347 3. Validation of the MC shear behaviour model with literature data

348 *3.1.Published data used for the validation step*

349 We consider four articles in the rock mechanics literature that present experimental direct
350 shear tests carried out in the validity conditions of the shear behaviour model developed
351 in this study. In these four studies, the joint roughness indicator (Z_2) ranges between 0
352 and 0.373 and joints were subjected to normal load ranging from 0.1 to 0.6-MPa during
353 the direct shear tests (Lee, Park, and Song 2014; Jang and Jang 2015; Li et al. 2018; Ram
354 and Basu 2019). Please note that the data from these studies were not used to develop the
355 numerical model previously described.

Ram and Basu (2019) studied the shear behaviour of unfilled natural rock joints with reference to the weathering grade of the joint. Due to the different weathering grade used by the authors, only seven direct shear tests results could be used (Table 4). These shear tests were carried out on smooth rock joints (Z_2 ranges from 0.057 to 0.130) under a normal stress of about 0.2-MPa.

Jang and Jang (2015) conducted more than 180 direct shear tests on rock joint replicas. Forty direct shear test results could be used directly in this research paper: Z_2 ranges from 0.082 to 0.351 and the normal stresses levels are 0.2 and 0.53-MPa MPa (Table 4).

From Lee, Park, and Song (2014), six direct shear tests results were extracted: Z_2 ranges from 0.142 to 0.253 and the normal stress levels range from 0.1 to 0.5-MPa (Table 4).

Lastly, in Li et al. (2018), only one direct shear test was conducted in the conditions presented above ($Z_2 < 0.373$ and the normal load from 0.1 to 0.6-MPa).

In brief, this amounts to fifty-four direct shear results selected from several published rock mechanics papers that were used to validate the shear behaviour model developed in this paper. The selected direct shear tests were carried out at various normal stress levels (from 0.1 to 0.53-MPa) on natural rock joints or on rock joint replicas that exhibited several levels of roughness (Z_2 ranging from 0.057 to 0.351). All of the selected papers gave the peak shear strength, whereas only eleven residual shear strengths were available.

3.2.Results

Table 4 and Figure 13 compare the experimental direct shear tests results from literature to the shear behaviour model blind-predictions. In Table 4, the relative difference between experimental results and model blind-predictions are also given.

Except for some cases that will be discussed, it appeared that the model developed is able to accurately predict the peak shear strength τ_{peak} of a natural rough rock joint subjected to low normal stress levels: a mean relative error of 12.0% is observed, and even 7.9% if some results are left out (Table 4). For example, joint N2000-J13 from the study of Jang and Jang (2015) exhibited an intermediate roughness (Z_2 = 0.21). Experimental peak shear strength was 0.412 MPa at 0.2MPa normal stress and 0.893 MPa at 0.53 MPa normal stress. In the exact same conditions of roughness, the shear behaviour model predicted a peak shear strength of 0.423 MPa and 0.943 MPa at 0.2 MPa and 0.53 MPa of normal stress. This represents a relative difference of 3% at 0.2 MPa normal stress and 6% at 0.53 MPa normal stress.

Regarding the residual shear strength (τ_r), a mean relative difference of 23% was obtained between the experimental results and the shear behaviour model blind-predictions (Table 4).

[TABLE 4 HERE]

[FIGURE 13 HERE]

3.3.Discussion

Regarding the peak shear strength (τ_{peak}), most of the model blind-predictions matched the experimental results although we observed some data with large differences (see dashed circles in Figure 13). In our opinion, the few large differences observed between the model blind-predictions and some very specific experimental data were linked to rock type. Indeed, during a direct shear test, a rock joint could exhibit different shear mechanisms such as sliding or shearing that can take place on the joint surface at the same time, depending on rock type, rock joint roughness and normal load (Rullière et al. 2020).

In our study, the shear behaviour model developed was based on granite joints, which are known to exhibit a "*slickenside to rough undulating roughness*" in accordance

406 with the ISRM (1978) description. In Rullière et al. (2020), the granite joints exhibited
407 mainly sliding mechanisms during the direct shear tests. On the other hand, in the study
408 of Jang and Jang (2015), the rock joints came from different rock types including granite
409 and schist joints, which are described being "*very rough and stepped*" in accordance with
410 the ISRM (1978). Very rough or stepped asperities will tend to gather the shear stresses
411 during a direct shear test, and schist joints will mainly be damaged by shearing
412 mechanisms. The reader should note that the direct shear tests conducted in (Lee, Park,
413 and Song 2014; Li et al. 2018; Ram and Basu 2019) were carried out on granite and gneiss
414 joints. In Jang and Jang (2015), as the rock type was not linked to the joint identification
415 code, it is therefore impossible to know which rock joint replica came from granite or
416 schists joints. Nevertheless, we attributed the large difference between the experimental
417 data and the model blind-predictions to the rock type (schist), as explained above. If the
418 specific large differences of Jang and Jang (2015) are excluded (see dashed circles in
419 Figure 13), the mean relative error between the experimental data from the rock
420 mechanics literature and the model blind-predictions is 7.9%.

421 Regarding the residual shear strength (τ_r), a mean relative difference of 23% was
422 obtained between the experimental results and the model blind-predictions (Table 4).
423 Although this mean relative difference is based on a few experimental results, as not all
424 the selected papers gave the residual shear strength, this gap between the experimental
425 data and the model blind-prediction can be explained by the following reasons:

426 • The model approach to predicting the residual shear strength is very conservative.
427 The shear stress decreases suddenly to its residual value once the peak is reached
428 whereas during an experimental direct shear test, the shear stress decreases
429 gradually to its residual value,

- Also, during this progressive shear stress decrease observed in the experimental tests, some shear stress jumps could be observed, very likely related to sheared material that interfered between the joint walls.

Finally, it appeared that the MC shear behaviour model integrating rock joint roughness was able to accurately predict the experimental peak shear strength of various direct shear tests published in the rock mechanics literature. For some specific cases, the blind-predictions were quite far from the experimental results, but in our opinion these differences can be explained by the rock type. Indeed, the shear behaviour model was developed using granite joints while some of the data presented were related to schist joints.

4. Application of the MC shear behaviour model to a gravity dam

Gravity dams are mainly exposed to shear mechanisms: under the combination of different actions, shearing can take place at the rock-concrete interface or at rock mass foundation joints. International gravity dam design guidelines suggest using the Mohr-Coulomb criterion to assess the shear strength of a rock joint of such structures (USBR 1987; US Army Corps of Engineers 1995; CFBR 2012; Federal Energy Regulatory Commission 2016).

Part 3 showed that the shear strength and behaviour of a rough rock joint subjected to low normal stresses could be accurately estimated by the numerical shear behaviour model developed, which takes into account joint roughness (developed in Part 2). In this Part 4, we wish to highlight: i) that the shear behaviour model developed previously could be used at the dam scale, and ii) the influence of the rock joint roughness on the shear behaviour of a gravity dam, subjected to different load cases.

4.1.Presentation of the numerical gravity dam model and hypothesis

The gravity dam studied is founded on a granitic rock mass from Canadian shield, intersected by three sets of joints that are prone to discontinuities in the displacement field, i.e. finite relative displacements across themselves. Among these sets, one is sub-horizontal and two sub-vertical, presenting dips of 16° N 0°, 80° N 0° and 82° N 180°, respectively. The joints of the same set are spaced according to a uniform distribution, whose standard deviations and mean values are given in Table 5. The persistence of the joints was considered as fully persistent (default preset). This agrees with the observations of the drillings carried out on the dam site, in the context of a dam founded on the Canadian shield where the persistence is generally very high.

All the joints exhibited the same roughness characteristics, described by a Z_2 value. In the following calculations, the Z_2 value was increased from zero (depicting a smooth joint) to 0.373 (depicting a very rough rock joint). It was also assumed that the rock mass joints are very long compared with the dam size and they can be considered as persistent at the numerical study scale. In other words, the joints we that the joints cut the entire rock foundation mass. There is therefore no increase in the length of the joints. On the other hand, the joints are free to open. The granite density was set to 2500 kg/m^3.

[TABLE 5 HERE]

The specifications of the case study gravity dam are:

- Height of 45m and an operating level of 41 m;
- The width at the head of the structure is 4 m;
- The upstream face is vertical, while the downstream batter (H/V) is 0.65;
- The width at the toe is 32 m.

The dam is fully made of concrete (density of 2350 kg/m^3) and it is assumed that its construction was of good quality: rock-foundation and construction interfaces were treated. In other words, excellent adhesion can be considered for concrete-concrete construction joints and rock-concrete interfaces. Therefore, relative displacements can only occur in the rock mass, along the rock joints described previously. For the sake of convenience, it was also assumed that the gravity dam was not equipped with any drainage system. Figure 14 shows a schematic view of the gravity dam modelled on its granitic rock mass foundation.

[FIGURE 14 HERE]

The numerical model is built using UDEC software (Itasca 2019) with a Discrete Element Method (DEM) approach. The DEM makes it straightforward to describe the discontinuity of displacements across joints, while a continuous-based FEM approach would require to adopt a more complex model, typically XFEM (Moës et al., 1999). In this DEM model, the particles are blocks of different sizes and shapes that come from three sets of discontinuities that cut the granitic massif. Numerical damping was used with a 0.8 coefficient and the time step was fixed at 30 μs to avoid divergence of the explicit dynamic scheme. The boundaries of the numerical model were fixed in all directions and located at a distance of at least five times the structure height to avoid any interferences.

Different load cases were considered:

(1) Normal Operating Conditions: the reservoir is filled;
(2) Extreme Conditions: the reservoir is filled and the dam is subjected to a seismic solicitation.

In Normal Operating Conditions, the dam is only subjected to mechanical actions related to the presence of water upstream of the structure (water pressure on the upstream

face of the dam, uplift). The reservoir is instantly filled with water from the natural foundation ground to the normal operating level (41 m of water upstream, 0 m of water downstream). The hydrostatic pressure field is imposed on the gravity dam rock foundation joints and assumed to be constant in time.

The seismic calculation is performed using a simple pseudo-static method, as suggested by French regulations. The values of the horizontal (a_h) and vertical acceleration (a_v) are: $a_h = 2.0$ m/s^2 and $a_v = 1.8$ m/s^2.

For the two loading cases considered, the analysis of the behaviour of the structure is carried out based on horizontal and vertical displacements of: i) the dam downstream face crest, and ii) the dam foundation at a depth of 3 m below the upstream toe.

4.2.Results and discussion

Table 6 shows the displacements recorded during the numerical modelling of a gravity dam subjected to load levels. From Table 6, it appears that the rock joint roughness has an important effect on the horizontal displacements recorded at the dam crest or in its foundation. However, the effect of rock joint roughness on the vertical displacements is not obvious.

For smooth rock foundation joints ($Z_2 = 0$), when the dam is filled and without seismic solicitation, the horizontal and vertical displacements recorded at the dam crest reach respectively a value of 17.2 mm and -0.74 mm. When seismic solicitation is applied, the displacements at the dam crest increase and reach the values of 24.5 mm for the horizontal displacement and 2.21 mm for the vertical displacement (Table 6).

For the rough rock foundation joints ($Z_2 = 0.373$), the horizontal displacements observed at the crest under normal operations and seismic conditions are reduced in comparison to smooth joints. Under normal operating conditions, the horizontal dam crest displacements reach the value of 11.00 mm maximum versus 17.2 mm for smooth joints,

i.e. a difference of 36% (Table 6). Under seismic conditions, the same trend can be observed: horizontal dam crest displacements reach a value of 19.00 mm versus 24.5 mm for smooth joints, i.e. a difference of 22% (Table 6). Figure 15 clearly shows that the horizontal displacements recorded at the dam crest (under normal operating and seismic conditions) decrease linearly when the rock joint roughness increases.

The largest displacements were observed at the crest of the structure; they are the consequence of displacements of the rock discontinuities located inside the rock mass foundation, as depicted in Figure 16. In Table 6 and Figure 17, it can also be seen that as the rock joint roughness increases, the horizontal displacement recorded below the dam upstream toe decreases linearly.

[TABLE 6 HERE]

[FIGURE 15 HERE]

[FIGURE 16 HERE]

[FIGURE 17 HERE]

Therefore, the application of the MC shear behaviour model integrating rock joint roughness to the gravity dam scale illustrates the important role of rock joint roughness in the shear behaviour of the dam. This influence of roughness was considered through the shear behaviour model input parameters. It appeared that displacement linearly decrease with an increase of rock foundation joint roughness (Z_2 value), either at dam crest or in its foundation (normal operation and extreme conditions).

Conclusion

The aim of this study was to develop a practical shear behaviour model, based on the Mohr-Coulomb model, which depicts the role of joint roughness on joints shear behaviour. The MC shear behaviour model integrating rock joint roughness included

551 constitutive stress-displacement laws. The model shear failure corresponded to the Mohr-
552 Coulomb criterion including apparent cohesion.

553 The shear behaviour model was developed based on more than thirty-five
554 experimental tests (direct shear tests and compression tests). Power laws that correlated
555 the joint roughness parameter Z_2 to the shear behaviour input parameter were developed
556 (calibration step, Part 2). The model was then validated by comparing its blind-
557 predictions to publish experimental data (validation step, Part 3). The results indicated
558 that the MC shear behaviour model integrating rock joint roughness was able to predict
559 the peak shear strength of an unbounded rock joint with an average relative error of 7.9%).
560 The shear behaviour model developed was found to be strongly influenced by the rock
561 type.

562 Lastly, the shear behaviour model developed was applied at full scale (gravity
563 dam) to highlight the role of rock joint roughness in dam shear behaviour. This practical
564 application exhibited that the higher the rock joint roughness (Z_2 value), the smaller the
565 displacements (either at the dam crest or in its foundations).

566 Regarding the perspectives of this work, it is important to recall that the MC shear
567 behaviour model integrating rock joint roughness is valid for specific conditions: a normal
568 load from 0.1 to 0.6-MPa and a roughness indicator Z_2 ranging from 0 to 0.373. Moreover,
569 the shear behaviour model developed takes into account the effects of joint roughness on
570 its shear strength and behaviour. However, the reader should know that other parameters
571 could also have strong effects (rock properties, interlocking, contact properties, the
572 presence of infilled materials in joints, etc.).

573 Future work will attempt to incorporate other shear behaviour / strength influence
574 parameters in the shear behaviour model developed. However, this task requires much
575 more data and implies launching new experimental and exhaustive studies. Finally, it is

576 important to note that the last part of this paper is intended to be only explanatory since
577 the tests were conducted at the laboratory scale. Thus, more work is required to use the
578 shear behaviour model developed accurately at a larger scale.

579 **Acknowledgments**

580 The authors are grateful to the National Sciences and Engineering Research
581 Council of Canada (NSERC), Hydro-Québec and INRAE (France) for funding the
582 project. We thank Danick Charbonneau and Ghislaine Luc for their technical help during
583 the experimental project.

584 **References**

585 Amitrano, D., and Schmittbuhl, J. 2002. “Fracture Roughness and Gouge Distribution
586 of a Granite Shear Band.” *Journal of Geophysical Research: Solid Earth* 107
587 (B12): 1–16. https://doi.org/10.1029/2002JB001761.

588 Bandis, S.C, Lumsden, A., and Barton, N.R. 1981. “Experimental Studies of Scale
589 Effects on the Shear Behaviour of Rock Joints.” *International Journal of Rock*
590 *Mechanics and Mining Sciences & Geomechanics Abstracts* 18 (1): 1–21.
591 https://doi.org/10.1016/0148-9062(81)90262-X.

592 Bandis, S.C., Lumsden, A.C., Barton, N.R. 1983. “Fundamentals of Rock Joint
593 Deformation.” *International Journal of Rock Mechanics and Mining Sciences &*
594 *Geomechanics Abstracts* 20 (6): 249–68. https://doi.org/10.1016/0148-
595 9062(83)90595-8.

596 Barton Nick, Shen Baotang. 2017. "Risk of shear failure and extensional failure around
597 over-stressed excavations in brittle rock". *Journal of Rock Mechanics and*
598 *Geotechnical Engineering.* Volume 9, Issue 2, April 2017, 210-225.

https://doi.org/10.1016/j.jrmge.2016.11.004

Barton, N., and V. Choubey. 1977. “The Shear Strength of Rock Joints in Theory and Practice.” *Rock Mechanics* 10 (1–2): 1–54. https://doi.org/10.1007/BF01261801.

Beer, A. J., D. Stead, and J. S. Coggan. 2002. “Technical Note Estimation of the Joint Roughness Coefficient (JRC) by Visual Comparison.” *Rock Mechanics and Rock Engineering* 35 (1): 65–74. https://doi.org/10.1007/s006030200009.

Buzzi, O, and D Casagrande. 2018. “A Step towards the End of the Scale Effect Conundrum When Predicting the Shear Strength of Large in Situ Discontinuities.” *International Journal of Rock Mechanics and Mining Sciences*, 2018. https://doi.org/10.1016/j.ijrmms.2018.01.027.

CFBR. 2012. “Recommandations Pour La Justification de La Stabilité Des Barrages-Poids.”

Chen Bing, Shen Baotang, Jiang Haiyang. 2022. "Shear behavior of intact granite under thermo-mechanical coupling and three-dimensional morphology of shear-formed fractures". *Journal of Rock Mechanics and Geotechnical Engineering*. https://doi.org/10.1016/j.jrmge.2022.04.006

Cundall, P. A., and J Lemos. 1988. “Numerical Simulation of Fault Instabilities with the Continuously-Yielding Joint Model.” In *PROCEEDINGS OF THE 2ND INTERNATIONAL SYMPOSIUM ON ROCKBURSTS AND SEISMICITY IN MINES*, edited by C Fairhurst. Minneapolis: Balkema Rotterdam. https://doi.org/10.1016/0148-9062(85)92069-8.

Duriez, J., Darve, F., and Donzé, F.-V.. 2011. “A Discrete Modeling-Based Constitutive

621 Relation for Infilled Rock Joints." *International Journal of Rock Mechanics and*
622 *Mining Sciences* 48 (3): 458–68. https://doi.org/10.1016/j.ijrmms.2010.09.008.

623 EPRI. 1990. "Uplift Pressures, Shear Strengths, and Tensile Strengths for Stability
624 Analysis of Concrete Gravity Dams."

625 Fan, Wenchen, Ping Cao, and Guodong Tang. 2018. "Experimental and Numerical
626 Study on the Damage Evolution of Random Rock Joint Surface During Direct
627 Shear Under CNL Condition." *Geotechnical and Geological Engineering* 37 (2):
628 975–83. https://doi.org/10.1007/s10706-018-0664-y.

629 Federal Energy Regulatory Commission. 2016. "Gravity Dams." In *Engineering*
630 *Guidelines for the Evaluation of Hydropower Projects*, 3.1–3.39.

631 Ghazvinian, A. H., A. Taghichian, Mahmoud Hashemi, and S. A. Mar'ashi. 2010. "The
632 Shear Behavior of Bedding Planes of Weakness Between Two Different Rock
633 Types with High Strength Difference." *Rock Mechanics and Rock Engineering* 43
634 (1): 69–87. https://doi.org/10.1007/s00603-009-0030-8.

635 Goodman, RE, RL Taylor, and TL Brekke. 1968. "A Model for the Mechanics of
636 Jointed Rock." *Journal of the Soil Mechanics and Foundation Division ASCE*
637 14:637–659.

638 Grasselli, G., and Egger, P. 2003. "Constitutive Law for the Shear Strength of Rock
639 Joints Based on Three-Dimensional Surface Parameters." *International Journal of*
640 *Rock Mechanics and Mining Sciences* 40 (1): 25–40.
641 https://doi.org/10.1016/S1365-1609(02)00101-6.

642 Hsiung, S.M., Ghosh, A., Ahola, M P., and Chowdhury, A.H. 1993. "Assessment of

643 Conventional Methodologies for Joint Roughness Coefficient Determination."
644 *International Journal of Rock Mechanics and Mining Sciences And* 30 (7): 825–29.
645 https://doi.org/10.1016/0148-9062(93)90030-H.

646 ISRM. 1978. "International Society for Rock Mechanics Commission on
647 Standardization of Laboratory and Field Tests. Suggested Methods for the
648 Quantitative Description of Discontinuities in Rock Masses." *International Journal*
649 *of Rock Mechanics and Mining Sciences and Geomechanics Abstracts* 15 (6): 319–
650 68. https://doi.org/10.1016/0148-9062(78)91472-9.

651 Ulusay, R. 2014. *The ISRM Suggested Methods for Rock Characterization, Testing and*
652 *Monitoring: 2007-2014*. Ed. Springer International Publishing.
653 https://doi.org/10.1007/978-3-319-07713-0.

654 Itasca. 2019. *UDEC - Universal Distinct Element Code - User Manual*. Minneapolis:
655 Itasca Consulting Group.

656 Jacobsson, L., Flansbjer, M., and Andersson, L. 2016. "Normal Loading and Shear
657 Tests on Rock Joints from Olkiluoto" 31 (June).

658 Jang, Hyun-Sic, and Bo-An Jang. 2015. "New Method for Shear Strength
659 Determination of Unfilled, Unweathered Rock Joint." *Rock Mechanics and Rock*
660 *Engineering* 48 (4): 1515–34. https://doi.org/10.1007/s00603-014-0660-3.

661 Kulatilake, P.H.S.W., Shou, G., Huang, T.H., and Morgan, R.M. 1995. "New Peak
662 Shear Strength Criteria for Anisotropic Rock Joints." *International Journal of Rock*
663 *Mechanics and Mining Sciences & Geomechanics Abstracts* 32 (7): 673–97.
664 https://doi.org/10.1016/0148-9062(95)00022-9.

665 Kumar, Rakesh, and Abhiram Kumar Verma. 2016. “Anisotropic Shear Behavior of
666 Rock Joint Replicas.” *International Journal of Rock Mechanics and Mining*
667 *Sciences* 90 (December): 62–73. https://doi.org/10.1016/j.ijrmms.2016.10.005.

668 Lee, Yong-Ki, Jung-Wook Park, and Jae-Joon Song. 2014. “Model for the Shear
669 Behavior of Rock Joints under CNL and CNS Conditions.” *International Journal*
670 *of Rock Mechanics and Mining Sciences* 70 (September): 252–63.
671 https://doi.org/10.1016/j.ijrmms.2014.05.005.

672 Li, Oh, Mitra, and Hebblewhite. 2016. “A Constitutive Model for a Laboratory Rock
673 Joint with Multi-Scale Asperity Degradation.” *Computers and Geotechnics* 72:
674 143–51. https://doi.org/10.1016/j.compgeo.2015.10.008.

675 Li, Yuanhui, Leibo Song, Quan Jiang, Chengxiang Yang, Chang Liu, and Bing Yang.
676 2018. “Shearing Performance of Natural Matched Joints with Different Wall
677 Strengths under Direct Shearing Tests.” *Geotechnical Testing Journal* 41 (2):
678 20160315. https://doi.org/10.1520/GTJ20160315.

679 Magsipoc, Earl, Qi Zhao, and Grasselli, G.. 2019. “2D and 3D Roughness
680 Characterization.” *Rock Mechanics and Rock Engineering*, no. 0123456789.
681 https://doi.org/10.1007/s00603-019-01977-4.

682 Marache, A. 2002. “Comportement Mécanique d’une Fracture Rocheuse Sous
683 Contraintes Normale et Tangentielle.” École Centrale des Arts et Manufactures
684 « École Centrale Paris ».

685 Moës, N., Dolbow, J. and Belytschko, T. 1999. "A finite element method for crack
686 growth without remeshing." *Int. J. Numer. Meth. Engng.* 46: 131-150,
687 https://doi.org/10.1002/(SICI)1097-0207(19990910)46:1<131::AID-

688 NME726>3.0.CO;2-J

689 Myers, N.O. 1962. “Characterization of Surface Roughness.” *Wear* 5 (3): 182–89.
690 https://doi.org/10.1016/0043-1648(62)90002-9.

691 Nouailletas, O., C. Perlot, P. Rivard, G. Ballivy, and C. La Borderie. 2017. “Impact of
692 Acid Attack on the Shear Behaviour of a Carbonate Rock Joint.” *Rock Mechanics*
693 *and Rock Engineering* 50 (6): 1439–51. https://doi.org/10.1007/s00603-017-1182-
694 6.

695 Oh, J, E J Cording, and T Moon. 2015. “A Joint Shear Model Incorporating Small-Scale
696 and Large-Scale Irregularities.” *International Journal of Rock Mechanics and*
697 *Mining Sciences* 76: 78–87. https://doi.org/10.1016/j.ijrmms.2015.02.011.

698 Patton, FD. 1966. “Multiple Modes of Shear Failure In Rock.” In *1st ISRM Congress*.
699 Lisbon: International Society for Rock Mechanics.

700 Ram, B. K., and A. Basu. 2019. “Shear Behavior of Unfilled-Planar Quartzitic Rock
701 Joints with Reference to Weathering Grade of Joint Surfaces.” *Rock Mechanics*
702 *and Rock Engineering* 52 (10): 4113–21. https://doi.org/10.1007/s00603-019-
703 01815-7.

704 Rullière, A., Rivard, P., Peyras, L., Breul, P. 2020. “Influence of Roughness on the
705 Apparent Cohesion of Rock Joints at Low Normal Stresses.” *Journal of*
706 *Geotechnical and Geoenvironmental Engineering* 146 (3): 1–15.
707 https://doi.org/10.1061/(ASCE)GT.1943-5606.0002200.

708 Rulliere, A., Rivard, P., Peyras, L., Breul, P. 2021. “Influence of Material Strength on
709 the Apparent Cohesion of Unbounded Gravity Dam Joints under Low Normal Stress.”

Journal of Geotechnical and Geoenvironmental Engineering 147(10). DOI: 10.1061/(ASCE)GT.1943-5606.0002608.

Sow, D., P. Rivard, L. Peyras, P. Breul, Z. A. Moradian, C. Bacconnet, and G. Ballivy. 2016. "Comparison of Joint Shearing Resistance Obtained with the Barton and Choubey Criterion and with Direct Shear Tests." *Rock Mechanics and Rock Engineering* 49 (8): 3357–61. https://doi.org/10.1007/s00603-015-0898-4.

Sow, D., Carvajal, C., Breul, P., Peyras, L., Rivard, P., Bacconnet, C., and Ballivy, G.. 2017. "Modeling the Spatial Variability of the Shear Strength of Discontinuities of Rock Masses: Application to a Dam Rock Mass." *Engineering Geology* 220: 133–43. https://doi.org/10.1016/j.enggeo.2017.01.023.

Tatone, Bryan S.A., and Grasselli, G. 2010. "A New 2D Discontinuity Roughness Parameter and Its Correlation with JRC." *International Journal of Rock Mechanics and Mining Sciences* 47 (8): 1391–1400. https://doi.org/10.1016/j.ijrmms.2010.06.006.

Tatone, Bryan S A, and Grasselli, G. 2013. "An Investigation of Discontinuity Roughness Scale Dependency Using High-Resolution Surface Measurements." *Rock Mechanics and Rock Engineering* 46 (4): 657–81. https://doi.org/10.1007/s00603-012-0294-2.

Tse, R, and Cruden, D.M. 1979. "Estimating Joint Roughness Coefficients." *International Journal of Rock Mechanics and Mining Sciences & Geomechanics Abstracts* 16 (5): 303–7. https://doi.org/10.1016/0148-9062(79)90241-9.

US Army Corps of Engineers. 1995. *Gravity Dam Design*. *USACE Engineer Manual*. 1st ed. Washington: DEPARTMENT OF THE ARMY U.S. Army Corps of

Engineers. http://oai.dtic.mil/oai/oai?verb=getRecord&metadataPrefix=html&identifier=ADA402909.

USBR. 1987. *Design of Small Dams*. Edited by A Water Resources Technical Publication. *UNITED STATES DEPARTMENT OF THE INTERIOR BUREAU OF RECLAMATION - A Water Resources Technical Publication*. 3rd ed.

Wang Luyu, Vuik Cornelis, Hajibeygi Hadi. 2022. "A stabilized mixed-FE scheme for frictional contact and shear failure analyses in deformable fractured media". E*ngineering Fracture Mechanics,* Vol. 267, 15 May 2022. https://doi.org/10.1016/j.engfracmech.2022.108427

Wang Luyu, Chen Weizhong, Tan Xuyan, Tan Xianjun, Yang Jianping, Yang Diansen & Zhang Xi. 2020. "Numerical investigation on the stability of deforming fractured rocks using discrete fracture networks: a case study of underground excavation". Bu*lletin of Engineering Geology and the Environment,* 79, 133–151. https://doi.org/10.1007/s10064-021-02233-2

Wang, Hu, and Hang Lin. 2018. “Non-Linear Shear Strength Criterion for a Rock Joint with Consideration of Friction Variation.” *Geotechnical and Geological Engineering* 36 (6): 3731–41. https://doi.org/10.1007/s10706-018-0567-y.

Xia, Cai-Chu, Zhi-Cheng Tang, Wei-Min Xiao, and Ying-Long Song. 2014. “New Peak Shear Strength Criterion of Rock Joints Based on Quantified Surface Description.” *Rock Mechanics and Rock Engineering* 47 (2): 387–400. https://doi.org/10.1007/s00603-013-0395-6.

Zhang Qi, Yan Xia, Li Zihao. 2022a. "A mathematical framework for multiphase

poromechanics in multiple porosity media". *Computers and Geotechnics.* Vol. 146, June 2022. https://doi.org/10.1016/j.compgeo.2022.104728

Zhang Qi, Wang Ze-Yu, Yin Zhen-Yu, Jin Yin-Fu. 2022b. "A novel stabilized NS-FEM formulation for anisotropic double porosity media". C*omputer Methods in Applied Mechanics and Engineering.* Vol. 401, Part B, 1 Nov. 2022, https://doi.org/10.1016/j.cma.2022.115666

Zhang, Xiaobo, Qinghui Jiang, Na Chen, Wei Wei, and Xixia Feng. 2016. "Laboratory Investigation on Shear Behavior of Rock Joints and a New Peak Shear Strength Criterion." *Rock Mechanics and Rock Engineering* 49 (9): 3495–3512. https://doi.org/10.1007/s00603-016-1012-2.

Zhao, J. 1997a. "Joint Surface Matching and Shear Strength Part A: Joint Matching Coefficient (JMC)." *International Journal of Rock Mechanics and Mining Sciences* 34 (2): 173–78. https://doi.org/10.1016/S0148-9062(96)00062-9.

Zhao, J. 1997b. "Joint Surface Matching and Shear Strength Part B: JRC-JMC Shear Strength Criterion." *International Journal of Rock Mechanics and Mining Sciences* 34 (2): 179–85. https://doi.org/10.1016/S0148-9062(96)00063-0.

Appendix A

Linear laws correlating the Z_2 value to the shear behaviour model input parameters.

$$K_N = 31.22 \cdot x + 68.14 \qquad R^2 = 0.96 \qquad (8)$$

$$K_S = 4.91 \cdot x + 1.96 \qquad R^2 = 0.77 \qquad (9)$$

$$C_{app\ peak} = 821.9 \cdot x - 28.5 \qquad R^2 = 0.88 \qquad (10)$$

$$\varphi_{peak} = 118.5 \cdot x + 28.06 \qquad R^2 = 0.96 \qquad (11)$$

779 $\varphi_{residual} = 89.6 \cdot x + 25.6$ $R^2 = 0.98$ (12)

780 $dN = 79.55 \cdot x + 0.26$ $R^2 = 0.99$ (13)

781 Exponential laws correlating the Z_2 value to the shear behaviour model input parameters.

782 $K_N = 15.87 \cdot e^{1.49 \cdot x} + 52.61$ $R^2 = 0.97$ (14)

783 $K_S = 0.257 \cdot e^{5.77 \cdot x} + 1.90$ $R^2 = 0.94$ (15)

784 $C_{app\ peak} = 56.64 \cdot e^{5.09 \cdot x} - 55.01$ $R^2 = 0.99$ (16)

785 $\varphi_{peak} = 1.164x10^4 \cdot e^{0.011 \cdot x} - 1.164x10^4$ $R^2 = 0.96$ (17)

786 $\varphi_{residual} = 1.081x10^4 \cdot e^{0.006 \cdot x} - 1.081x10^4$ $R^2 = 0.96$ (18)

787 $dN = 1.809x10^4 \cdot e^{0.0041 \cdot x} - 1.809x10^4$ $R^2 = 0.98$ (19)